Palaeogeography, Palaeoclimatology, Palaeoecology 524 (2019) 118–136

Contents lists available at ScienceDirect

Palaeogeography, Palaeoclimatology, Palaeoecology

journal homepage: www.elsevier.com/locate/palaeo

Terrestrial and marginal-marine record of the mid-Cretaceous Oceanic Anoxic Event 2 (OAE 2): High-resolution framework, carbon isotopes, CO_2 and sea-level change

Jiří Laurin[a,*], Richard S. Barclay[b], Bradley B. Sageman[c], Robin R. Dawson[d], Mark Pagani[d,1], Mark Schmitz[e], Jeffrey Eaton[f], Francesca A. McInerney[g], Jennifer C. McElwain[h]

[a] Institute of Geophysics, Academy of Sciences of the Czech Republic, Boční II/1401, Praha 4, Czech Republic
[b] Department of Paleobiology, Smithsonian Institution, National Museum of Natural History, 10th & Constitution Avenue NW, Washington, D.C. 20560-0121, USA
[c] Department of Earth & Planetary Sciences, Northwestern University, 2145 Sheridan Road Technological Institute, Evanston, IL, 60208, USA
[d] Department of Geology and Geophysics, Yale University, New Haven, CT 06520, USA
[e] Department of Geosciences, Boise State University, 1910 University Drive, Boise, USA
[f] P.O. Box 231, Tropic, UT 84776, USA
[g] Department of Earth Sciences, University of Adelaide, Adelaide, SA, Australia
[h] Department of Botany, Trinity College Dublin, College Green, Dublin 2, Ireland

ARTICLE INFO

Keywords:
Cenomanian
Cretaceous
Paleoclimate
Carbon cycle
Orbital eccentricity
Milankovitch cycles

ABSTRACT

Oceanic Anoxic Event 2 (OAE2; c. 94.5–93.9 Ma) offers insight into the mechanisms of past climate change linked to organic productivity and carbon sequestration. It has been studied extensively, but the vast majority of data come from marine records, thus providing an incomplete view of past climate dynamics. Here we integrate new high-resolution data and published records on depositional environments, the carbon-isotope composition of bulk organic carbon ($\delta^{13}C_{org}$) and plant cuticles ($\delta^{13}C_{cut}$), and stomatal-index values, a proxy for pCO_2, in well-preserved terrestrial through marginal-marine archives of the initial phase of OAE2. The study area is located on the western margin of the Western Interior Seaway (southwestern Utah). Age constraints are based on a new U-Pb bentonite age and correlation to an orbitally calibrated interval of the Bridge Creek Limestone. *n*-Alkane abundance suggests predominance of terrestrial contributions to bulk organic carbon for most samples. Despite similarities between carbon-isotope variations and transgressive-regressive shoreline movements, it is argued that $\delta^{13}C_{org}$ and $\delta^{13}C_{cut}$ are not strongly affected by local variables. A series of negative, ~2‰ carbon-isotope excursions is identified and attributed to changes in the size and isotopic value of the atmospheric CO_2 reservoir. The temporal spacing of these anomalies (80–120 kyr) is consistent with changes in insolation modulated by orbital eccentricity. A systematic, phase-shifted relationship between the negative carbon-isotope excursions and transgressive increments further suggests a link between carbon-cycle perturbations and meter-scale sea-level change on the 100-kyr time scale. A conceptual model involving insolation-controlled aquifer charge/discharge and biomass burial/degradation in the monsoonal belt is proposed. The framework presented here is available to facilitate further research on the interplay of terrestrial and oceanic carbon reservoirs during OAE2.

1. Introduction

The Late Cenomanian to earliest Turonian OAE2 was an episode of organic-carbon sequestration from the ocean-atmosphere reservoir in a world characterized by extremely high surface temperatures (> 35 °C; O'Brien et al., 2017) and elevated concentrations of greenhouse gases in the atmosphere (Berner, 2006; Beerling et al., 2011). The event is marked by enhanced marine productivity, anoxia and organic-carbon burial (e.g., Schlanger and Jenkyns, 1976; Arthur et al., 1988) fueled by nutrient fluxes from submarine volcanism (Snow et al., 2005; Turgeon and Creaser, 2008; Adams et al., 2010; Flögel et al., 2011b; Du Vivier et al., 2014) and/or terrestrial sources (Frijia and Parente, 2008; Blättler et al., 2011; Pogge von Strandmann et al., 2013). Although the major carbon sinks are centered in the low-latitude Atlantic (review in

* Corresponding author.
E-mail address: laurin@ig.cas.cz (J. Laurin).
[1] Deceased.

https://doi.org/10.1016/j.palaeo.2019.03.019
Received 30 October 2018; Received in revised form 11 March 2019; Accepted 12 March 2019
Available online 21 March 2019
0031-0182/

Trabucho Alexandre et al., 2010), the resulting ^{13}C-enrichment of the carbon cycle has been recognized globally in the carbon-isotope composition of marine carbonate (Scholle and Arthur, 1980), marine organic matter (Arthur et al., 1988) and wood fragments preserved in proximal marine settings (Takashima et al., 2010).

Available data suggest a primarily oceanic causal pathway for initiation of the event with ties to atmospheric and terrestrial feedbacks including altered weathering rates (e.g., Pogge von Strandmann et al., 2013) and fluctuations in the atmospheric concentration of CO_2 (e.g., Sinninghe Damsté et al., 2008; Barclay et al., 2010). Regional fluctuations in hydrological balance are documented by palynomorph assemblages (van Helmond et al., 2014, 2015; Heimhofer et al., 2018) and changes in charcoal abundance (Baker et al., 2019, in press). The information on atmospheric and terrestrial processes is, however, greatly underrepresented in the current OAE2 database. The detailed structure of atmospheric perturbations, their relationship to sea-level change and the possible role of terrestrial carbon reservoirs remain unknown due to limited time control and the fragmentary nature of non-marine records. The Naturita Formation (formerly Dakota Formation) of southwestern Utah can help fill this gap. It formed along the western margin of the Western Interior Seaway as part of the Sevier foredeep, and preserves an expanded terrestrial and marginal-marine record of the initial phase of OAE2 (Elder et al., 1994; Tibert et al., 2003; Laurin and Sageman, 2007). Correlation to the Bridge Creek Limestone and its astronomical time scale (Sageman et al., 2006; Meyers et al., 2012a) provides unprecedented temporal control (Laurin and Sageman, 2007), now confirmed by a new astrochronologic analysis of the SH#1 core (Jones et al., 2019), which was drilled in southern Utah, the geographic focus of this study.

The aim of this paper is to (1) present new carbon-isotope measurements of bulk organic carbon and plant cuticles from terrestrial, marginal-marine and offshore sites of the OAE2 interval in southwestern Utah, (2) combine these data with published carbon-isotope and stomatal-index results (Barclay et al., 2010), and (3) integrate the isotopic and stomatal-index dataset with a sedimentological, sequence-stratigraphic and chronostratigraphic framework established in Laurin and Sageman (2007). In addition to providing an updated interpretation of the onset of OAE2 in the study area, the results point to a close relationship between changes in atmospheric chemistry and short-term sea-level change. Finally, the stratigraphic and geochemical data offer a high-resolution framework that can be employed in further research of the non-marine expression of OAE2.

2. Depositional setting

The study area is located at the western margin of the Cretaceous Western Interior Seaway (WIS), in the foredeep of the Sevier fold-and-thrust belt (Figs. 1 and 2). Proximity to the Sevier thrust resulted in relatively high subsidence and sedimentation rates during the Late Cenomanian (> 100 m/Myr; Laurin and Sageman, 2007).

Terrestrial and paralic strata are exposed in the western part of the Markagunt plateau (Big Hill locality in Cedar Canyon, and two localities in the Kanarra Mountains). Eastward, towards the Paunsaugunt and Kaiparowits Plateaus, the paralic interval grades to offshore fines. A similar succession spanning terrestrial through open-marine strata is found up-section in the Markagunt Plateau (Fig. 3). The lower part of the study interval in Cedar Canyon and the Kanarra Mountains is formed by fluvial siliciclastics (channels, crevasse splays) and interfluve paleosols; this interval is of Middle and Late Cenomanian age and was defined as the Middle Member of the Dakota Formation in previous studies (e.g., Elder et al., 1994; see below for proposed revision of lithostratigraphic nomenclature). The non-marine succession passes upward to a paralic interval (Upper Member, Dakota Formation), most of which corresponds to the ammonite zone *Sciponoceras gracile*, i.e., the initial phase of OAE2 (Fig. 3). These strata record a wide range of marginal-marine and shallow-marine environments (e.g., lagoons, washover fans, tidal inlets, upper shoreface) interbedded with coals and paleosols. They are overlain by shoreface and offshore deposits of the uppermost Cenomanian *Neocardioceras juddii* Zone through Lower Turonian *Mammites nodosoides* Zone (Tibert et al., 2003; Laurin and Sageman, 2007). The depositional facies, transgressive-regressive context and indices for relative sea-level falls are discussed in Laurin and Sageman (2007).

3. Methods

3.1. Sampling

Samples for carbon-isotope analysis were collected from terrestrial and marginal-marine strata of two sections in the Kanarra Mountains area (KM2 and Laverkin) and one section in the Cedar Canyon area (Big Hill; Fig. 2; geographic coordinates are provided in Table S4). The same localities served as reference points for the chronostratigraphic framework and interpretation of transgression and regression (Laurin and Sageman, 2007). Hence, the isotope samples can be tied directly to the facies, genetic sequences and numerical ages interpreted previously. Bulk samples were collected from discrete horizons (2–5 cm thick) within every available fine-grained facies interval.

3.2. Cuticle extraction from bulk samples

Dispersed fossil leaf cuticle fragments were macerated from bulk samples following a three step procedure of hydrochloric acid (HCl), tetrasodium pyrophosphate decahydrate ($Na_4P_2O_7 \times 10\ H_20$), and hydrofluoric acid (HF). For details see Text S1.1.

3.3. Carbon isotope ratios

The procedures of sample preparation and carbon-isotope measurement are described in Text S1.2. Sample data is expressed in per mil notation (‰) relative to the Vienna Pee Dee Belemnite (VPDB) standard. Mean instrumental error was < 0.17‰; standard deviation ± 0.19‰. Mean bulk sample reproducibility was better than 0.24‰, with a standard deviation of ± 0.25‰. Samples with total organic carbon (TOC) contents below 0.15 wt% exhibited poor reproducibility and were therefore excluded from further analysis.

3.4. Lipid extraction and characterization

The extremes of medium-term excursions in bulk $\delta^{13}C_{org}$ were analyzed for *n*-alkane abundance in order to identify the controls on $\delta^{13}C_{org}$ signature (Dataset S9). Sample preparation and analysis are described in the supplementary Text S1.3.

Dominance of shorter chained *n*-alkanes (*n*-C_{15} to *n*-C_{19}) indicates a greater input from marine bacterial and algal sources (Clark and Blumer, 1967), while terrestrial higher plant input is dominated by longer chained *n*-alkanes (*n*-C_{25} to *n*-C_{33}; Rieley et al., 1991). To characterize the average chain length (ACL), where A_n refers to the area under the peak of carbon-chain length *n*, we use the following definition.

$$ACL = \sum (A_{15-33} \times 15 - 33) / \sum A_{15-33} \quad (1)$$

The thermal maturity of organic matter was qualitatively assessed using the Carbon Preference Index (CPI) of the *n*-alkanes as defined by Bray and Evans (1961) and modified by Marzi et al. (1993):

$$CPI_{total} = ((\sum odd\ C_{15-31}) + (\sum odd\ C_{17-33}))/(2 \times \sum even\ C_{16-32}) \quad (2)$$

$$CPI_{terr} = ((\sum odd\ C_{25-31}) + (\sum odd\ C_{27-33}))/(2 \times \sum even\ C_{26-32}) \quad (3)$$

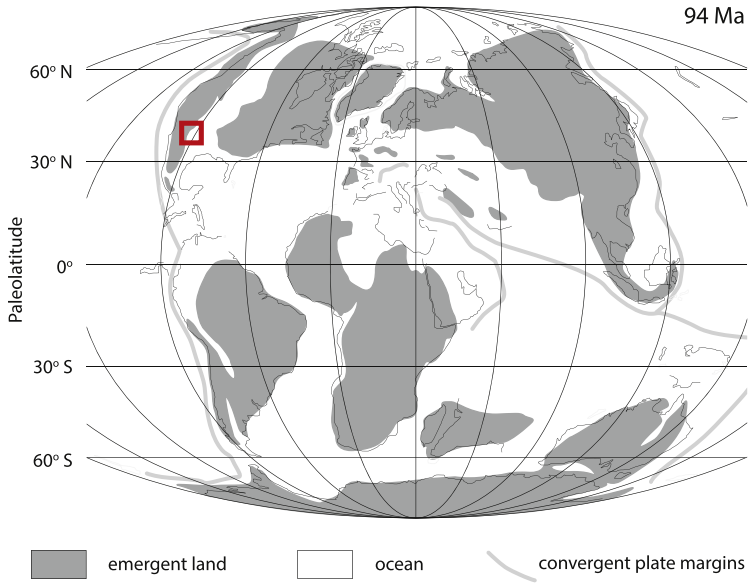

Fig. 1. Paleogeography of the Late Cretaceous (~94 Ma; after Scotese, 2001). Study area is highlighted.

CPI values above one indicate an odd-over-even predominance and original plant-derived signatures (Bush and McInerney, 2013; Liu and Liu, 2016), whereas lower values, approaching one, indicate petrogenic signatures. The distinction between aquatic and terrigenous plant sources can be made using the terrigenous/aquatic ratio (TAR) index, with values higher than 1 suggesting more input from terrestrial higher plants (Meyers, 1997).

$$TAR = \frac{C_{27} + C_{29} + C_{31}}{C_{15} + C_{17} + C_{19}} \quad (4)$$

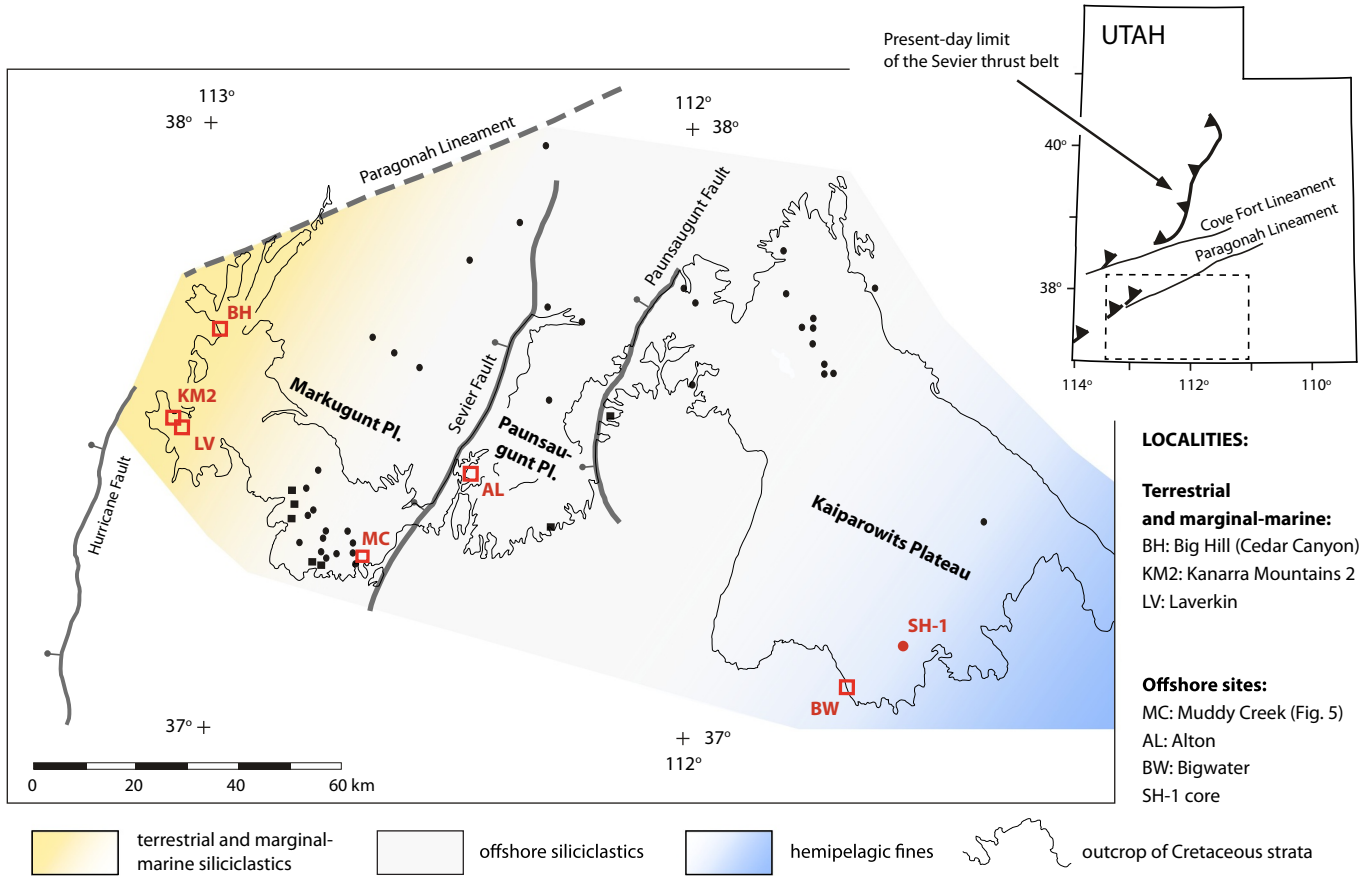

Fig. 2. Location map of the study area; modified from the Geologic map of Utah (Hintze, 1980). Localities discussed in this paper are shown in red. Black circles and rectangles denote boreholes and outcrops examined in a previous study (Laurin and Sageman, 2007). Position of structural features after Picha (1986). Barbs on upthrown hanging wall, and bars with balls on downthrown hanging wall. (For interpretation of the references to colour in this figure legend, the reader is referred to the web version of this article.)

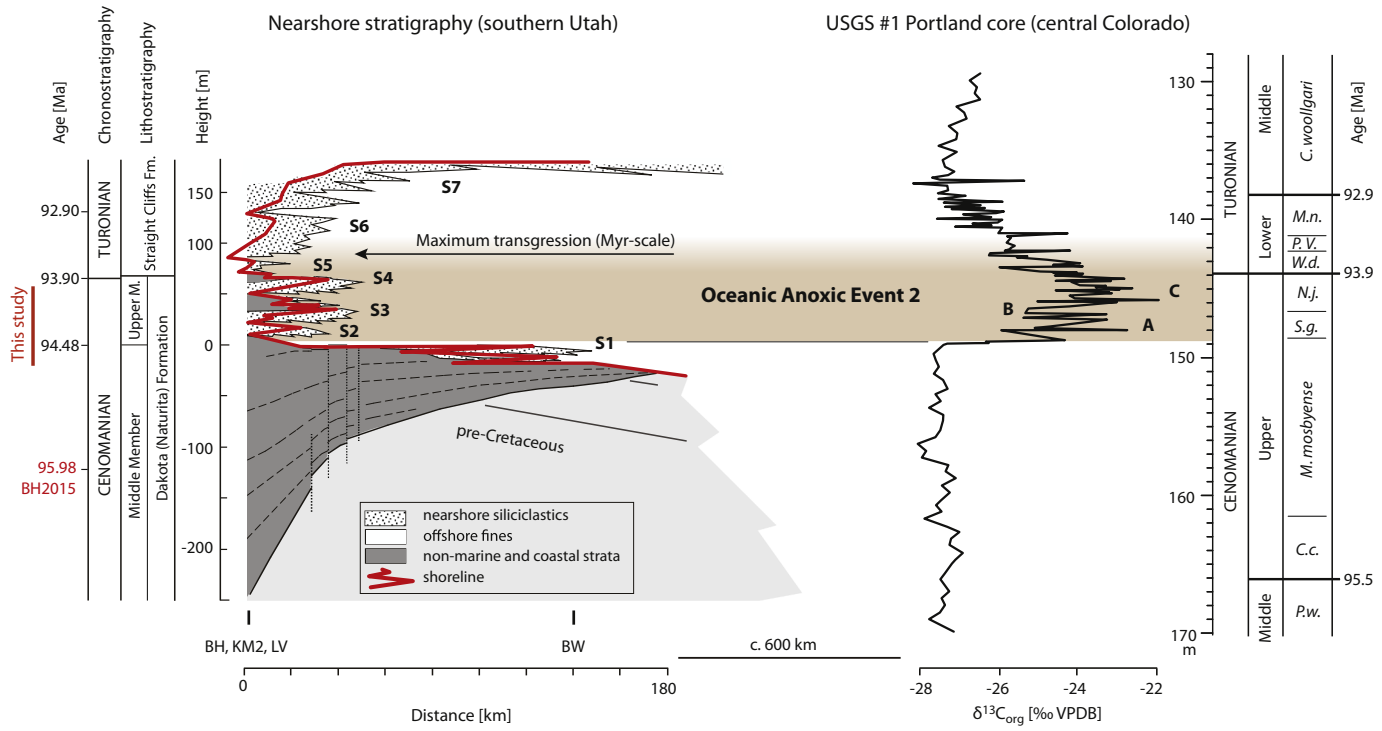

Fig. 3. Simplified stratigraphy of the study interval. Nearshore stratigraphy and medium-term genetic sequences (S1–S7) after Laurin and Sageman (2007). Portland core data are adopted from Sageman et al. (2006) and Joo and Sageman (2014). OAE2 phases "A", "B" and "C" after Pratt (1985). Stage and substage boundaries after Ogg et al. (2012), and floating age of the onset of OAE2 after Sageman et al. (2006) and Ma et al. (2014) (see Table 1). BH2015 = bentonite dated in this study. Chronostratigraphic zones: *M.m* = *Metoicoceras mosbyense* Zone, *S.g.* = *Sciponoceras gracile* Zone, *N.j.* = *Neocardioceras juddii* Zone, *W.d.* = *Watinoceras devonense* Zone; *P.V.* = *Pseudaspidoceras flexuosum* and *Vascoceras birchbyi* Zones, *M.n.* = *Mammites nodosoides* Zone, *C. woollgari* = *Collignoniceras woollgari* Zone, *C.c.* = *Calycoceras canitaurinum* Zone, *P.w.* = *Plesiacanthoceras wyomingense* Zone.

3.5. Radioisotopic dating

Carefully selected zircon fragments from a bentonite layer located 118 m beneath the base of the Upper Member of the Dakota Formation (BH2015; Figs. 3 and 4) were analyzed for U-Pb ages in the Isotope Geology Laboratory of the Boise State University. Details are provided in the supplementary Text S1.4 and Dataset S1.

3.6. Terminology

In a recent paper, Carpenter (2014) proposed that the lithostratigraphic term "Dakota Formation" was not appropriate for use in the study area and should be replaced by "Naturita Formation." In this paper, we prefer to retain use of the term "Dakota Formation" in order to better facilitate reference to previous research, which is fundamental to data integration.

The transgressive-regressive context of the study interval is based on recognition of "short-term" (tens of kyr), "medium-term" (~100-kyr) and "long-term" (Myr-scale) genetic sequences (Laurin and Sageman, 2007). The "medium-term" sequences are labeled S1 through S7 for informal purposes (Fig. 3). The time scale of "medium-term" sequences is comparable to the time scale of $\delta^{13}C_{org}$ anomalies discussed in this paper. The negative phases of these "medium-term" $\delta^{13}C_{org}$ anomalies are labeled "–a0", "–a1", "–a2" and "–a3", while the positive excursions are labeled "+a1", "+a2", "+a3" and "+a4" (Fig. 4).

4. Results

4.1. Stratigraphic framework

The Big Hill site in the Cedar Canyon area provides the most complete exposure, and is therefore considered the reference section for this study. Correlation of nearby sections in the Cedar Canyon area and between Cedar Canyon and Kanarra Mountains is based on analogies in facies associations and sequence stratigraphic relationships, aided by marker bed correlation (e.g., bentonites, the Culver coal zones and other distinct facies, such as fossiliferous "marls" described by Tibert et al., 2003, from the immediate vicinity of the Cenomanian/Turonian boundary, meter levels 70–77 in Fig. 4). The stratigraphic framework mostly follows the framework established in Laurin and Sageman (2007). Minor updates are applied to the base of paralic sedimentation at the KM2 site, which is reinterpreted (shifted 2.7 m lower) based on new data from an improved outcrop exposure (Figs. 4 and S1). Carbon-isotope data suggest that OAE2 starts above the base of the paralic strata (see Section 5.2).

Towards the Kaiparowits Plateau, along the depositional dip, the onset of paralic sedimentation is correlated to a prominent transgressive surface at the top of unit 6A of Uličný (1999). The overlying unit 6B backsteps relative to 6A, and is interpreted as coeval with the lowermost part of the transgressive tract of sequence S1 at Big Hill. Offshore strata above unit 6B (Tropic Shale) are correlated using bentonites, marlstone marker beds and biostratigraphic horizons (Elder et al., 1994; Laurin and Sageman, 2007; Fig. 5).

A detailed correlation of pre-OAE strata between the Big Hill reference section and localities in the Kaiparowits Plateau (Cottonwood Canyon, Wahweap Wash and Bald Knoll Mine; Uličný, 1999; Barclay et al., 2010) is hampered by the lack of suitable correlation markers in the non-marine succession. For this reason we avoid incorporating previously published $\delta^{13}C_{org}$ data from the Kaiparowits Plateau in the composite $\delta^{13}C_{org}$ log. Stomatal-index data from these localities are presented (Dataset S10), but their timing relative to samples from Big Hill and KM2 should be considered with an additional level of uncertainty (Text S2).

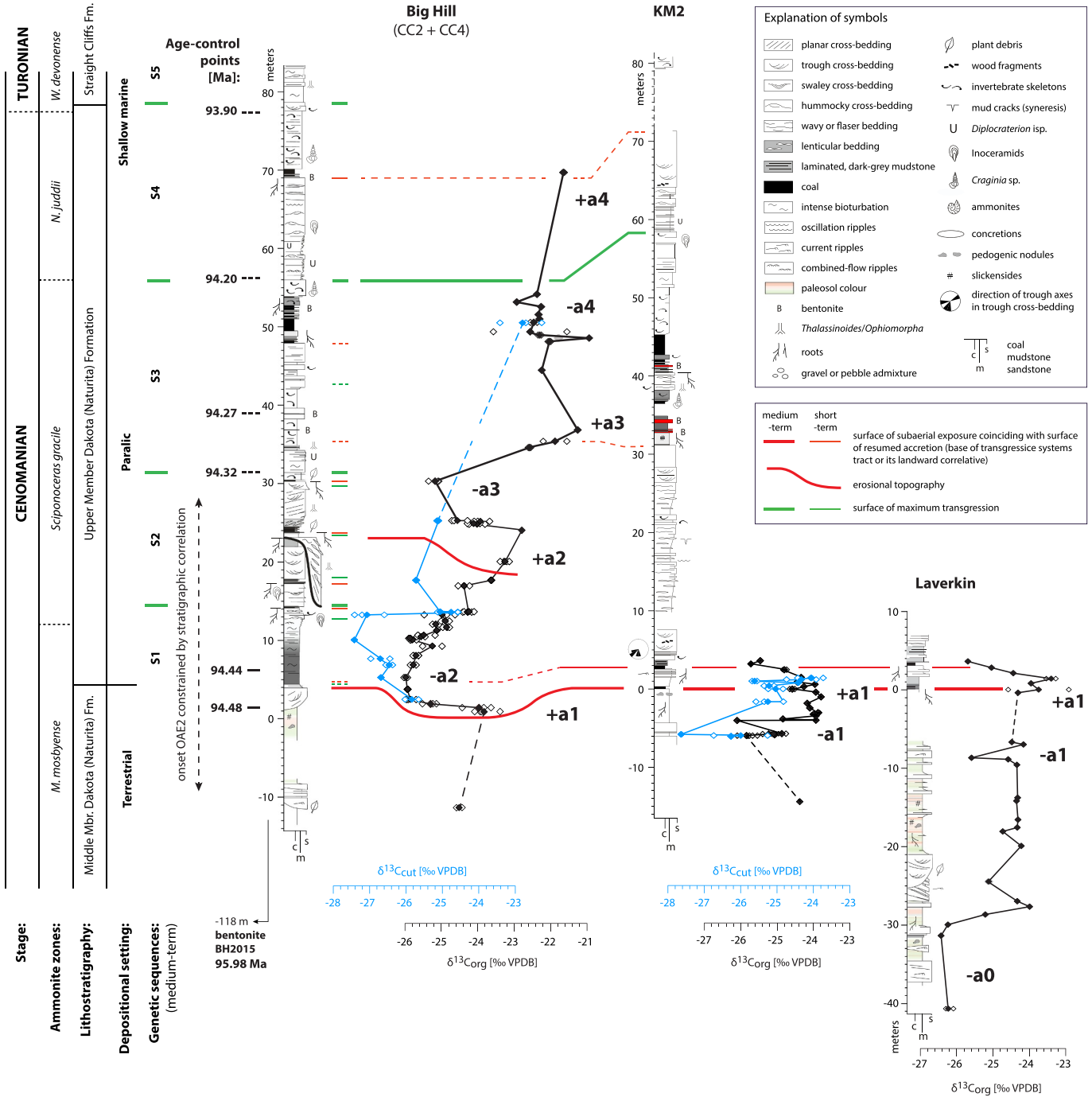

Fig. 4. Lithology, carbon-isotope composition of bulk organic carbon ($\delta^{13}C_{org}$; black data points) and carbon-isotope composition of cuticles ($\delta^{13}C_{cut}$; blue data points) from terrestrial and marginal-marine sections; SW Utah. See Fig. 2 for location. The Big Hill section is a composite of profiles CC2 and CC4 of Laurin and Sageman (2007). Open symbols: individual measurements; filled symbols: stratigraphic mean. Samples with TOC < 0.15% are not shown. Correlation to major bentonites, limestone marker beds and the onset of *N. juddii* Zone after Laurin and Sageman (2007). The base of Turonian after Tibert et al. (2003). Additional details including TOC data are presented in Fig. S1. (For interpretation of the references to colour in this figure legend, the reader is referred to the web version of this article.)

4.2. Age constraints

The primary chronostratigraphic constraint is provided by the Cenomanian-Turonian (C/T) boundary, corresponding to the first appearance of *Mytiloides puebloensis* in the transgressive tract of sequence S4 in Cedar Canyon (Tibert et al., 2003; section CC9 of Laurin and Sageman, 2007). Paralic strata underlying the C/T boundary are linked to the astronomical time scale of the Bridge Creek Limestone (Sageman et al., 2006; Meyers et al., 2012a; Ma et al., 2014) using biostratigraphic and marker-bed correlation in outcrops and well logs (Laurin and Sageman, 2007; see also Elder et al., 1994; Table 1).

In order to anchor the base of the study interval, we present radioisotopic (U-Pb) ages of zircons from a bentonite layer located within the non-marine succession, 118 m beneath the base of the paralic unit at Big Hill, Cedar Canyon (sample BH2015; Fig. 4). These zircons bear a Middle Cenomanian age of 95.98 Ma (± 0.12 Myr total uncertainty; Text S1.4).

A total of eight age control points is applied to the study interval at

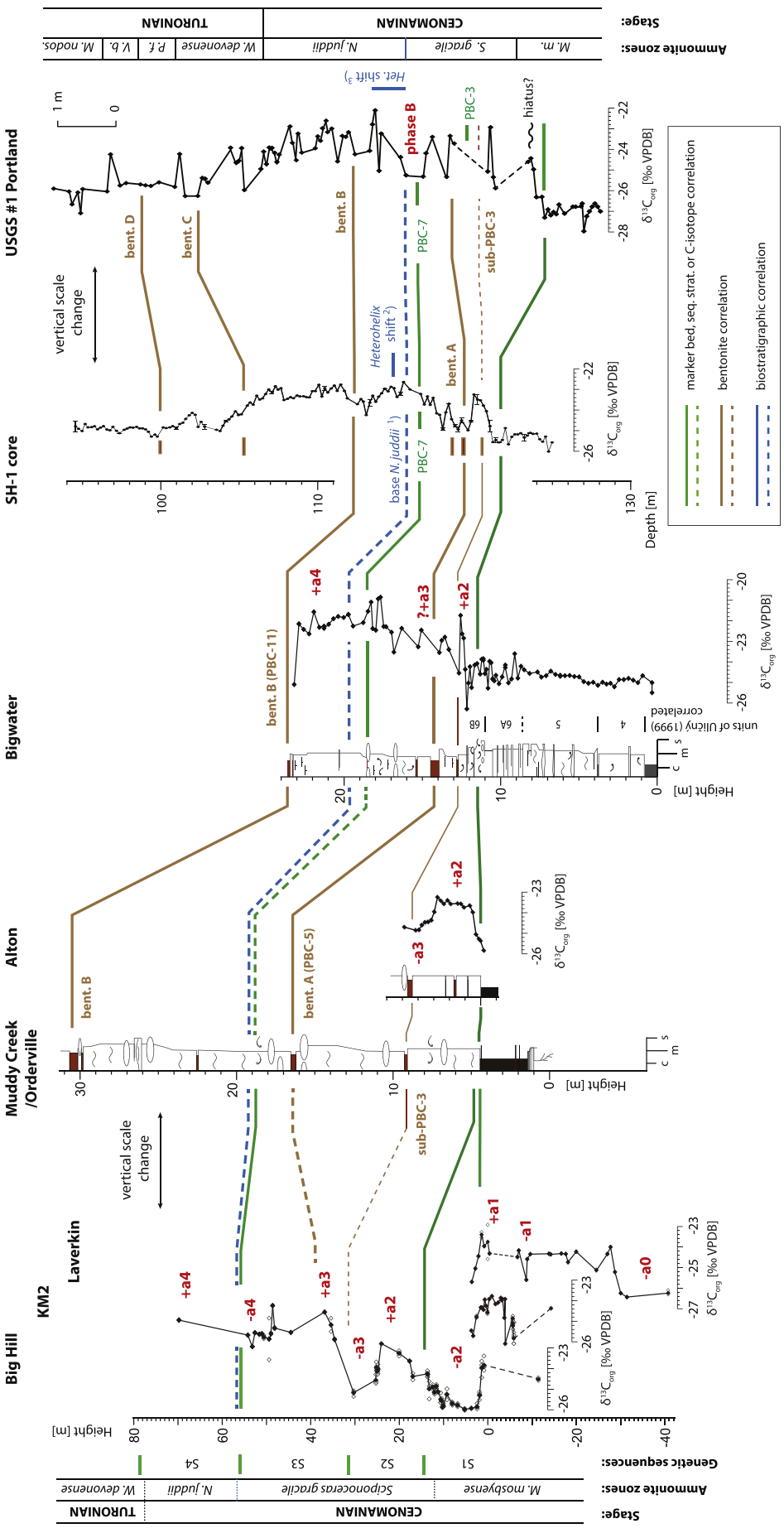

Fig. 5. Correlation of the marginal-marine record with offshore and hemipelagic sites. See Fig. 2 for location. Marker bed designation after (Elder and Kirkland, 1985). Bentonite "sub-PBC-3" has not been included in the original suite of marker beds. However, it forms a prominent marker in SW Utah, traceable in well logs and outcrops. It was therefore labeled informally by Laurin and Sageman, 2007 (see their Figs. 9 through 11) based on its position beneath limestone marker bed PBC-3 in Canyon City, central Colorado (Hattin, 1985). Location in the USGS Portland core is approximate; the layer has not been recognized in the core. Sources of data: USGS #1 Portland core lithology, $\delta^{13}C$ and chronostratigraphy after Sageman et al. (2006); SH-1 core after Jones et al. (2019); Muddy Creek/Orderville modified after Elder (1991); Bigwater, Alton, Big Hill, KM2 and Laverkin: this study. [1]) Base of the *N. juddii* Zone at Bigwater and SH-1 are based on correlation to the nearby Wahweap Wash (U1) and KPS sections of Elder (1989, 1991) and Elder et al. (1994). [2]) *Heterohelix* shift in the SH-1 core after Jones et al. (2019). [3]) Base of the *N. juddii* Zone and *Heterohelix* shift in the Portland core are based on correlation to the Global Boundary Stratotype Section at Pueblo (Leckie, 1985; Kennedy et al., 2005; Sageman et al., 2006).

Table 1
Age control points used in this study.

Age control point	Stratigraphic level at Big Hill	Numerical age	Uncertainty (numerical age only)	Floating age relative to base Turonian	Floating age relative to bentonite A	Age model
	[m]	[Ma]	[Myr]	[Myr]	[Myr]	[Ma]
Base TURONIAN	77	93.90[a]	+0.07/−0.09	0		93.90
Bentonite B	~73	94.07[a]	+0.16/−0.15			94.07
Base *N. juddii* Zone	56			0.30[b]		94.20
Bentonite A	39	94.27[a]	+0.16/−0.17	0.37[b]	0	94.27
Bentonite sub-PBC-3[g]	31			0.42[b]		94.32
Base positive CIE (onset OAE2)	6.5				0.17[c]	94.44
Base negative CIE (precursor)	1.6				0.21[c]	94.48
Bentonite KJ08142	–[d]	94.88[e]	± 0.11			94.88
Bentonite KJ08143	–[d]	95.07[e]	± 0.12			95.07
Bentonite BH2015	−118	95.98[f]	± 0.12			95.98

[a] Meyers et al. (2012a); USGS #1 Portland core.
[b] Sageman et al. (2006); USGS #1 Portland core.
[c] Ma et al. (2014); Aristocrat Angus core.
[d] Applies to the Kaiparowits Plateau only; detailed correlation to Big Hill uncertain.
[e] Barclay et al. (2015); Henrieville section.
[f] This study; Big Hill section.
[g] Correlated from Canyon City (Hattin, 1985; see Fig. 11 of Laurin and Sageman, 2007).

Big Hill (Table 1). The ages of individual carbon-isotope and stomatal-index samples are estimated using a linear interpolation between these points. For additional details see Text S2.

4.3. Carbon isotope ratios

4.3.1. Terrestrial and marginal-marine sites

Isotope data from the bulk organic carbon cover 40 m of non-marine strata of the Middle Member of the Dakota Formation and 70 m of paralic strata of the Upper Member of the Dakota Formation. These results are presented along with previously published $\delta^{13}C_{org}$ data from the paralic unit (Barclay et al., 2010) and new $\delta^{13}C_{cut}$ data from the upper part of non-marine succession at KM2 and lower part of the paralic unit at Big Hill (Fig. 4). All data are listed in Datasets S2 through S6.

The lower, non-marine part of the study interval exhibits relatively low $\delta^{13}C_{org}$ values ranging mostly between −26.5 and –23.5‰ (Fig. 4). Two intervals with ^{13}C-depleted values (~−26‰) are labeled informally "–a0" and "–a1" (Fig. 4). Five samples from the KM2 site are extremely depleted (−35 to −28‰; Dataset S3). These values are, however, restricted to carbon-poor paleosols (< 0.3% TOC) and not reproduced in coeval strata at Laverkin, suggesting a local origin possibly related to extreme microbial degradation in soils (Wynn, 2007). As a result, these data are not considered relevant and are excluded in figures and discussion.

A long-term increase in $\delta^{13}C_{org}$ indicative of OAE2 starts above the onset of marginal-marine facies. It is best documented at Big Hill, where the long-term change proceeds in three increments (excursions "+a2", "+a3" and "+a4") punctuated by prominent negative excursions "–a2", "–a3", and (less pronounced) "–a4" (Fig. 4).

Cuticle $\delta^{13}C$ values are typically depleted in ^{13}C relative to bulk samples. Where available, they follow a similar pattern as $\delta^{13}C_{org}$, reproducing negative anomalies "–a1" and "–a2", and positive anomalies "+a1" and "+a2". Minor differences are observed in the timing of $\delta^{13}C$ anomaly "–a2", where the minimum in $\delta^{13}C_{cut}$ postdates minimum in $\delta^{13}C_{org}$ (Fig. 4).

4.3.2. Offshore sites

Offshore sites examined here include the Alton coal mine and Bigwater (Fig. 2). The onset of OAE2 at these localities coincides with a landward shift in facies, which is represented by a superposition of offshore mudstones over coal (Alton) and shoreface siliciclastics (Bigwater).

Pre-OAE2 values are captured at Bigwater, where they occupy a relatively narrow range between −25.2 and –23.8‰ (Fig. 5). The base of offshore strata is marked by a brief negative excursion (correlative to "–a2"). Above this level, $\delta^{13}C_{org}$ values start rising in two distinct increments separated by a minor negative excursion (correlative to "–a3"; Fig. 5). Maximum $\delta^{13}C_{org}$ values (−20.8‰) are found in the upper part of sequence S3, beneath the base of *N. juddii* Zone. The Alton and Bigwater data are listed in Datasets S7 and S8.

4.4. n-Alkane abundance

Most sediment samples show carbon preference index (CPI_{terr} and CPI_{total}) values > 1.5, suggesting that the *n*-alkanes in this section are representative of original sources of organic matter (Bray and Evans, 1961; Fig. 6). However, the material at ~20 m (isotope excursion "+a2") has a CPI closer to 1, suggesting the organic matter at this level is possibly more thermally degraded (Bray and Evans, 1961) or that *n*-alkanes at this level are dominated by those from a marine microbial source (Clark and Blumer, 1967). Despite a minor overall decrease in ACL moving up section (26–28 in the lower terrestrial interval to 24–27 in the upper paralic interval), long chain *n*-alkanes are abundant throughout, with *n*-C_{27} and *n*-C_{29} dominating in most of the samples. An exception is the sample at 5.2 m where *n*-C_{17} is the dominant peak. The lower ACL and TAR at this level suggest that organic matter in this part of the section is dominated by algae rather than terrestrial plants (Fig. 6; Meyers, 1997; Xing et al., 2011). In the sample located in the negative anomaly "–a3" (~30 m; Fig. 6), *n*-C_{31} co-eluted with a presumed contaminant based on its disproportionate peak height (> 80% of total peak areas), and thus *n*-C_{31} was not included in the calculations, which would bias metrics towards more marine and aquatic signatures, rather than terrestrial ones. Even so, this sample TAR value of ~6 indicates a terrestrial origin.

4.5. Integration of stratigraphic and carbon-isotope data

Carbon-isotope data presented here and in a previous study (Barclay et al., 2010) were collected from a wide range of terrestrial, marginal-marine and marine environments. Sedimentation rates in the marginal marine succession are inherently much more variable then

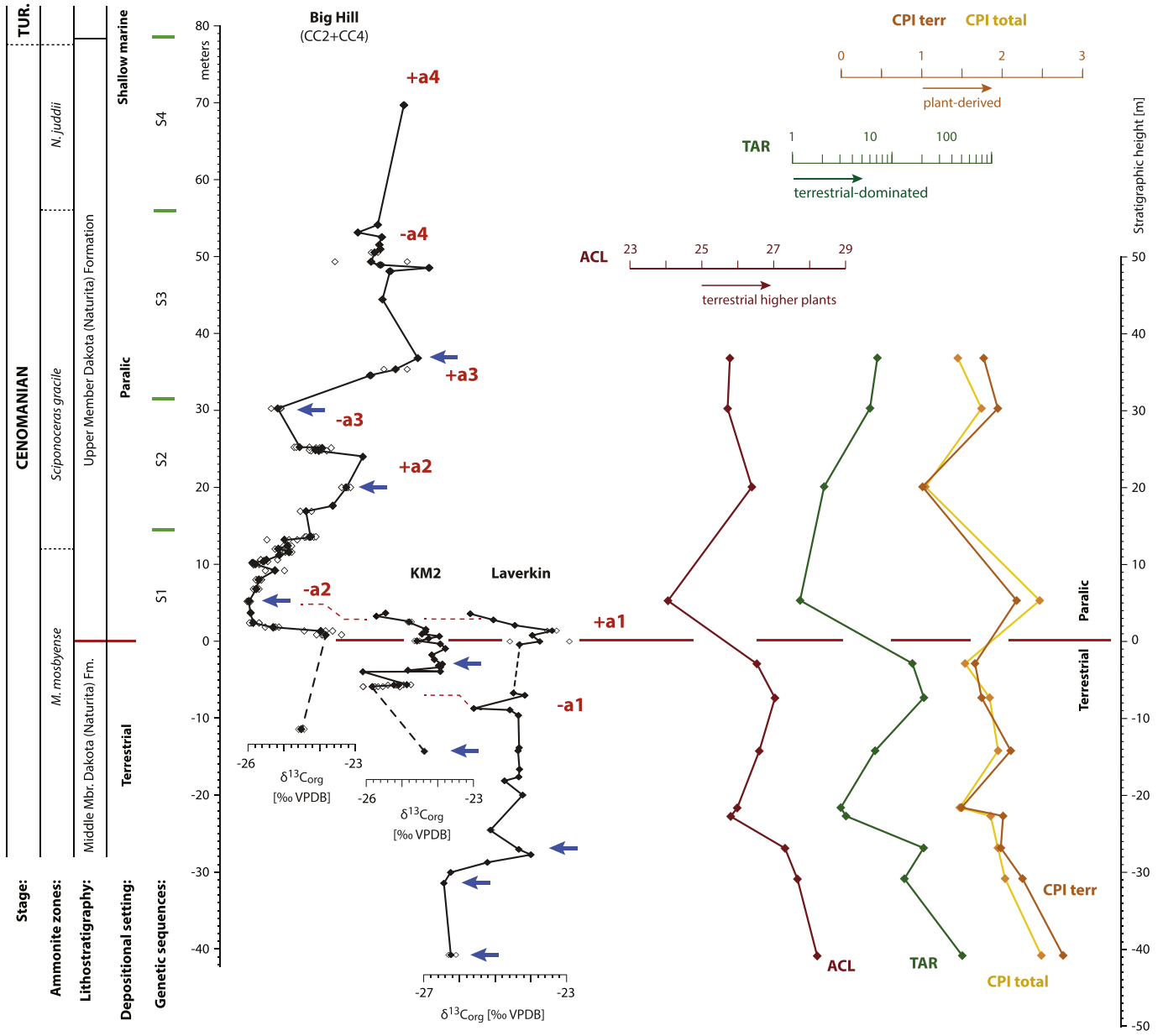

Fig. 6. Summary of organic-geochemistry results; level of samples is indicated by blue arrows. CPI = carbon preference index; ACL = average chain length; TAR = terrigenous/aquatic ratio. (For interpretation of the references to colour in this figure legend, the reader is referred to the web version of this article.)

sedimentation rates in offshore and hemipelagic sites that have provided most of the OAE2 record to date. On the long-term scale, the marginal-marine sedimentation was aggradational to weakly retrogradational suggesting that accommodation generally kept pace with (and later outpaced) sediment input. During short-term sea-level falls, however, the accommodation space was limited resulting in non-deposition and erosion. The geochemical and paleobotanical sampling (Barclay et al., 2010, and this study) are therefore biased towards transgressive facies, which form most of the study succession. In order to consider the asymmetry in sample distribution and evaluate the role of depositional environments in the $\delta^{13}C_{org}$ signature, each sample is linked to the transgressive-regressive context and equipped with a reference to the enclosing lithofacies (Dataset S2 and Table S1).

The data integration reveals a trend of increasing ^{13}C depletion with increasing marine influence in the depositional facies (Figs. 4 and 7). This pattern is further highlighted by similarities between $\delta^{13}C_{org}$ variations and transgressive-regressive shoreline movements in the study area (Fig. 8). A detailed look at the individual sequences, however, suggests that the two records are offset relative to each other. First, $\delta^{13}C_{org}$ maxima of anomalies "+a1" and "+a2" postdate evidence for regressive erosion and the onset of base-level rise in sequences S1 and S2. Second, the anomaly "–a2" predates the maximum transgression at the top of sequence S1 (Figs. 4 and 8; other extremes are not sampled to a sufficient detail). In other words, negative $\delta^{13}C_{org}$ excursions occupy relatively narrow intervals within transgressive systems tracts. Cuticle $\delta^{13}C$ data support these relationships, although the offset is less distinct in the anomaly "–a2" (Fig. 4). These observations argue against a local bias in $\delta^{13}C_{org}$, because local control would likely produce an in-phase correlation between $\delta^{13}C_{org}$ and environmental indicators. The relative timing suggests that $\delta^{13}C_{org}$ excursions and depositional changes were controlled by different pathways, although both ultimately linked to one primary forcing (as indicated by similarities in their pace; see Section 5.6).

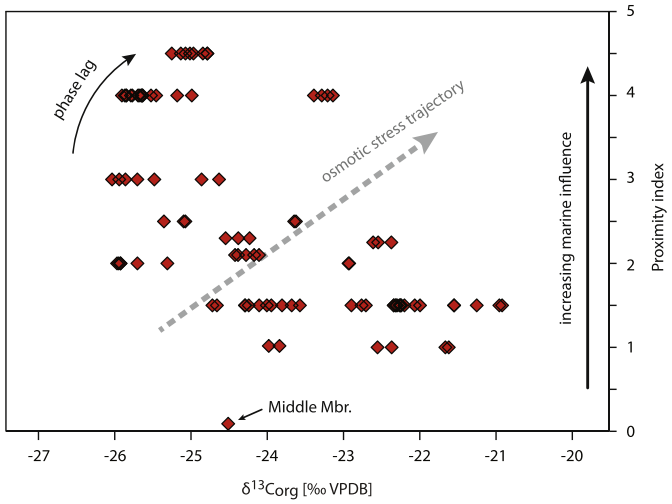

Fig. 7. Scatter plot of $\delta^{13}C_{org}$ vs. proximity index for the Upper Member of the Dakota Formation at Big Hill. The proximity index is based on facies analysis and is an arbitrary measure of the location of individual samples along the terrestrial-marine gradient (0 = terrestrial; 5 = offshore).

5. Discussion

5.1. Origin of $\delta^{13}C$ variability

The carbon-isotope composition of bulk organic carbon is a composite $\delta^{13}C$ signature of the ocean-atmosphere reservoir and the effects of physiological fractionation related to the source of organic material (Hayes, 1993). Biological and environmental factors potentially masking the global carbon-isotope signature are discussed below and in Table 2.

5.1.1. Source of organic matter

The prime concern in any marginal marine setting is mixing of terrestrial and marine materials in the bulk sample. Given 3 to 4‰ fractionation differences between terrestrial and marine organics in the Cretaceous (e.g., Dean et al., 1986; Gröcke, 2002), the negative excursions "–a1", "–a2" and "–a3" could be linked to an influx of marine organics during transgressions. To evaluate this possibility, we develop a simple linear mixing model assuming −25 to −27‰ composition of the coeval marine organics (based on data from the Portland and Angus cores; Sageman et al., 2006; Ma et al., 2014) and –23 to −24‰ composition of the background terrestrial material (based on values preceding the negative excursions in the marginal-marine setting, localities Big Hill and KM2). This model would require a switch from purely terrestrial to marine-dominated (63 to 100%) source to replicate each of the negative anomalies (see Table S2). *n*-Alkane indices from a sample located in the anomaly "–a2" (Fig. 6), would be consistent with such an explanation. However, this $\delta^{13}C$ anomaly is reproduced in $\delta^{13}C_{cut}$, although with a later timing of the minimum $\delta^{13}C$ value (Fig. 4). In addition, $\delta^{13}C_{org}$ variations in this interval are closely followed by changes in the stomatal index proxy for pCO_2 (Barclay et al., 2010; Fig. 8). We conclude that a contribution from marine organic source might be responsible for the earlier culmination of "–a2" in $\delta^{13}C_{org}$ relative to $\delta^{13}C_{cut}$. It is not, however, the principal control on the anomaly itself. Further explanation is sought in the terrestrial plant matter.

5.1.2. Carbon-isotope discrimination in plants

Changes to environmental conditions during plant growth can affect the photosynthetic efficiency of the carbon fixing enzyme Ribulose-1,5-bisphosphate carboxylase oxygenase, commonly referred to as RuBisCO. This alters the amount of fractionation that occurs during photosynthesis such that the final isotopic value of the plant tissue can change without any change to the atmospheric isotopic value (Arens et al., 2000; Jahren et al., 2008). $\delta^{13}C$ values for C_3 plants have a median isotopic value of about −27‰ in the modern world (Marshall et al., 2007). Variation in the isotopic value around the median depends on the balance between diffusive supply and enzymatic demand for CO_2 by RuBisCO, governed by Eq. (5), originally introduced by Farquhar et al. (1982):

$$\delta^{13}C_{leaf} = \delta^{13}C_{atm} - a - (b - a)\, c_i/c_a \quad (5)$$

where, a is the fractionation during diffusion into the stomatal pore, b is the fractionation associated with carbon dioxide fixation (27‰), and c_i/c_a is the ratio of intercellular to ambient concentrations of CO_2. Stomata close partially, reducing stomatal conductance, which affects diffusion of both CO_2 into the leaf and water out of the leaf. Water flux is reduced in proportion to the amount that stomatal conductance is reduced. The photosynthetic rate is also lowered by stomatal closure, but not in the same proportional relationship as for transpiration. This forces the internal reservoir of CO_2 to become enriched in ^{13}C (due to decreased c_i/c_a), ultimately shifting the isotopic composition of the resulting plant tissue towards more enriched values. Prolonged stomatal opening has the opposite effect of stomatal closure, as this increases c_i/c_a, creating a relatively more depleted isotopic value (Marshall et al., 2007). Differences in biological control of stomatal function also influence c_i/c_a, which has an effect on ^{13}C discrimination. There is a broad evolutionary difference between spore bearing and seed bearing plants which have higher c_i/c_a values and lower c_i/c_a values, respectively (Porter et al., 2017). Adaptation by the plant over time via modification of stomatal aperture size will also influence diffusion and thereby influence fractionation at the stomatal pore (Steinthorsdottir et al., 2012).

Depending upon the environmental variable, plant tissue can either become depleted or enriched in ^{13}C as a result of changes in c_i/c_a, by the processes explained above, thus affecting the isotopic value of the plant (summarized in Cernusak et al., 2013). The environmental and biological variables potentially affecting $\delta^{13}C$ signatures in the study interval are discussed in Table 2. Despite similarities between $\delta^{13}C$ variations and transgressive-regressive facies shifts, the arguments listed in Table 2 suggest that the medium-term isotope anomalies cannot be readily attributed to the local conditions. Instead, the relationship may indicate a link to a common primary forcing.

Based on the high degree of correspondence between the stomatal proxy record for pCO_2 and carbon isotopes, it is possible that CO_2 concentration is a mitigating factor. Although a compilation of published data on plant tissues grown under pCO_2 values below 1300 ppm shows no relationship between the amount of discrimination by plants and the level of pCO_2 (Beerling, 1996; Arens et al., 2000; Kohn, 2016), more recent studies suggest increasing ^{13}C enrichment with decreasing pCO_2 (Schubert and Jahren, 2012; Franks et al., 2014; Porter et al., 2017; Hare et al., 2018). Hence, the fractionation response to pCO_2 change might have enhanced the primary isotopic response of plant tissue to a $\delta^{13}C$ change of the atmospheric reservoir.

5.2. Onset of OAE2 in the marginal-marine record

The onset of OAE2 is constrained broadly by the onset of marine transgression at the base of the Dakota Formation. A detailed physical correlation is, however, hampered by a condensed interval in the offshore segment of sequence S2 (Laurin and Sageman, 2007). The highest possible correlative level is defined by the bentonite "sub-PBC-3", which postdates the onset of OAE2 by approximately 120 kyr (Laurin and Sageman, 2007). This marker bed is readily traceable in well logs, where it overlies the regressive package of sequence S2 (see Fig. 9 of Laurin and Sageman, 2007) and hence the positive excursion "+a2" (Fig. 5). This correlation places the excursion "+a3" securely within OAE2. The onset of the positive $\delta^{13}C$ shift related to OAE2 should be

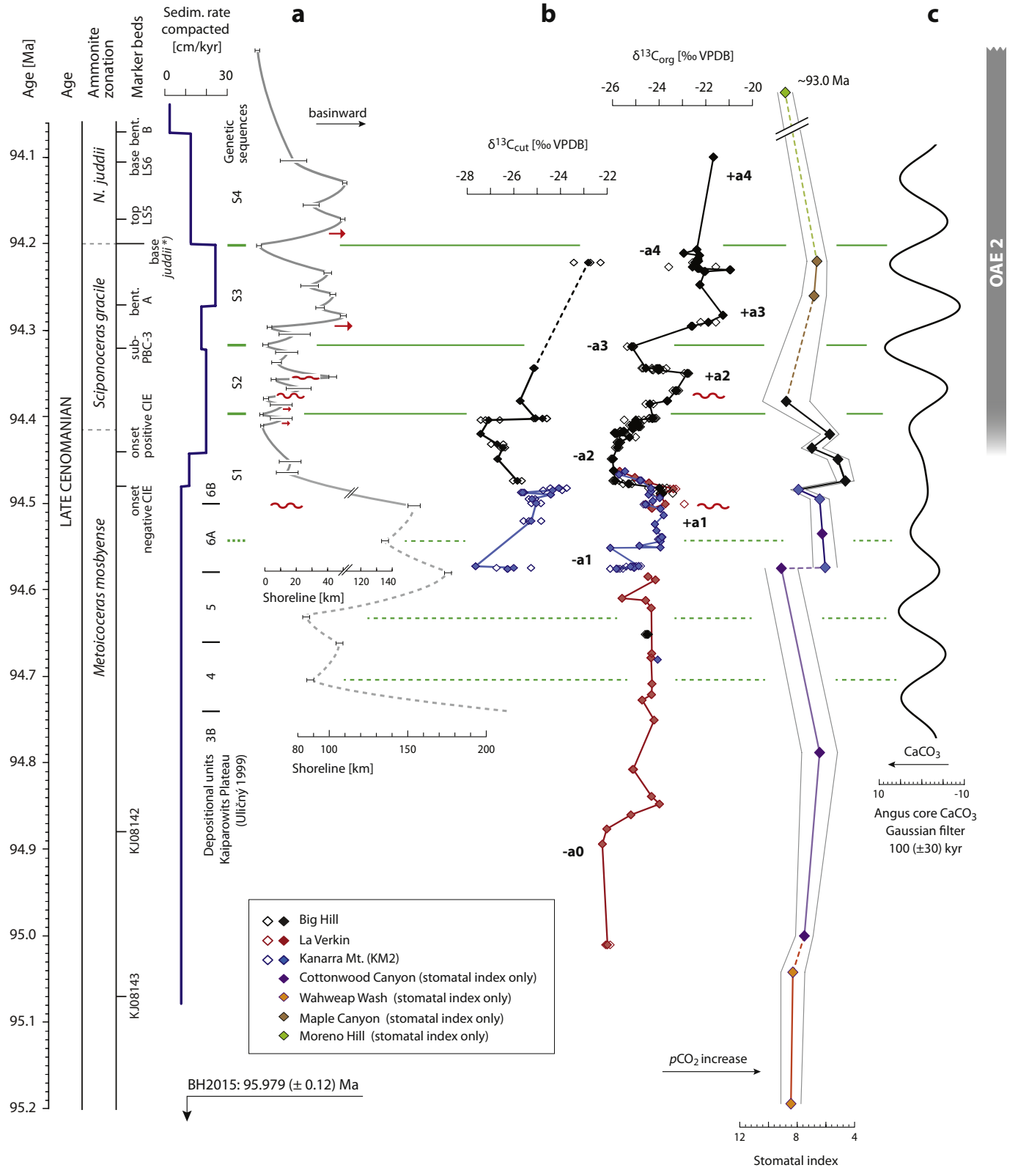

(caption on next page)

Fig. 8. Time-domain representation of the transgressive-regressive history, $\delta^{13}C_{org}$, $\delta^{13}C_{cut}$ and stomatal-index data. (a) Shoreline movements along a northwest-southeast transect (grey) and average sedimentation rates (blue). Error bars indicate uncertainty in the location of transgressive and regressive maxima. Sedimentological indices for relative sea-level falls are indicated by wavy lines (subaerial erosion and pedogenesis) and red arrows (abrupt basinward shifts in facies; see Laurin and Sageman, 2007, for details). Transgressive-regressive changes in the *M. mosbyense* Zone after Uličný, 1999 (his units 4 through 6B). Markers KJ08142 and KJ08143 refer to bentonites dated by Barclay et al. (2015) in the Kaiparowits Plateau. *) *N. juddii* Zone has been delineated as an assemblage zone, in the Western Interior Basin; its onset predates the first appearance of the ammonite *Neocardioceras juddii* (Elder, 1991; Elder et al., 1994; Kennedy et al., 2005; see also Fig. 11). CIE = carbon-isotope excursion of OAE2. (b) Composite plots of $\delta^{13}C_{cut}$, $\delta^{13}C_{org}$ and stomatal index. Individual data points are shown by open symbols. Filled symbols indicate stratigraphic mean. Stomatal-index data are modified after Barclay et al. (2010). Grey margins indicate standard deviation (Dataset S10). (c) Bandpassed ~100 kyr signature from Angus core $CaCO_3$ data (Ma et al., 2014). (For interpretation of the references to colour in this figure legend, the reader is referred to the web version of this article.)

therefore delineated by the excursion "+a1" or "+a2".

Using a preliminary suite of carbon-isotope data, Barclay et al. (2010) placed the onset of OAE2 at the base of excursion "+a1". Additional sampling, however, suggests that the excursion "+a1" does not rise above background $\delta^{13}C$ values characterizing the lower part of the study interval (Figs. 4 and 8). The overlying excursion "+a2" provides a better candidate for the onset of positive $\delta^{13}C$ anomaly of OAE2, although the amplitude is still relatively small owing partly to erosion during relative sea-level fall of sequence S2. The negative excursion "–a2" is then correlated to a minor negative shift recognized at the base of the OAE2 interval in the Angus core (Ma et al., 2014).

5.3. Terrestrial vs. marine signatures of OAE2

Both pre-OAE2 and OAE2 values of $\delta^{13}C_{org}$ become progressively more negative (^{13}C depleted) towards the basin center, consistent with a change from terrestrial to marine sources of organic carbon. Considering that typical terrestrial pre-OAE2 values of $\delta^{13}C_{org}$ range between −24 and –25‰ (Fig. 4), the peak OAE2 excursion recorded in the terrestrial organic carbon is comparable in its magnitude to the OAE2 excursion in marine organic carbon (3–4‰; Fig. 5). The internal structure of the terrestrial $\delta^{13}C$ record, however, differs from the marine signature. In spite of similarities in the incremental structure of the onset of OAE2 (e.g., Iona-1 core - Fig. 10; Eastbourne - Fig. 11), the negative excursions "–a2" and "–a3" are developed preferably in the terrestrial organics. On the other hand, a "trough" recognized in both organic and carbonate isotopes in marine sections of Colorado ("phase B" of Pratt, 1985), Eastbourne (Paul et al., 1999; Tsikos et al., 2004), and other sites, does not have a robust counterpart in southwestern Utah (Figs. 5, 11). We stress that a correlation error is unlikely, because the isotope "phase B" is tightly constrained by bentonite and limestone marker beds in addition to biostratigraphy (base of *N. juddii* Zone and *Heterohelix* shift; Fig. 5).

The absence of "phase B" (Pratt, 1985) or the "trough" in the marginal-marine record of southwestern Utah might be related to undersampling in an interval dominated by organic-poor sandstones (Fig. 4). A minor negative shift beneath the base of *N. juddii* Zone, labeled "–a4", is a possible expression of the globally recognized anomaly. "Phase B" is also absent from offshore strata of Bigwater and the SH-1 core (Fig. 5). Since these sites received organic material from both terrestrial and marine sources, it is assumed that variations in the terrestrial vs. marine carbon ratio combined with transgressive

Table 2
Possible controls on $\delta^{13}C_{org}$ and $\delta^{13}C_{cut}$ in the study interval.

Control	Reference	Relevance to study interval
Sample processing	Barral et al. (2015)	Samples were processed equally using HCl that has been shown not to influence $\delta^{13}C$ values, and concentrated HF, which gives consistent $\delta^{13}C$ mean values, despite potentially increasing variance (Barral et al., 2015).
Mixing of terrestrial and marine organics	Fractionation differences, e.g., Dean et al. (1986); Gröcke (2002)	Lower ACL and TAR in "–a2" suggests marine contribution. However, "–a2" is reproduced in $\delta^{13}C_{cut}$ and mirrored by stomatal-index change. N-alkane indices in anomalies "–a1" and "–a3" do not suggest increased marine influence.
Carbon degradation, pedogenesis	Wynn (2007)	Cuticles are well-preserved, display cellular detail. A lack of negative correlation between $\delta^{13}C$ and TOC (Fig. 9). Paleosol samples with low TOC (< 0.15%) were excluded from $\delta^{13}C$ analysis.
Carbon-isotope discrimination in plants:		
Water stress and low relative humidity	Ehleringer et al. (1986); Toft et al. (1989); Wright et al. (1994)	Can result in ^{13}C enrichment; however, no indications for aridity in positive $\delta^{13}C$ anomalies; elevated fire indicators (charcoal) only in negative anomaly "–a2" (predate increase in $\delta^{13}C_{cut}$ and acceleration in $\delta^{13}C_{org}$; Baker et al., 2019)
Physiological drought in anoxic bogs		Can result in ^{13}C enrichment; excluded based on the lack of positive covariance between $\delta^{13}C$ and organic carbon contents (Fig. 9).
Osmotic stress	Guy et al. (1980); Aucour et al. (2008)	Can result in ^{13}C enrichment; however, positive $\delta^{13}C$ anomalies are found preferably in regressive facies that should correspond to reduced saltwater influence (Fig. 7).
Position in the canopy	Bush et al. (2017)	Two palisade parenchyma cell layers increase preservation potential of sun leaves (Martin and Juniper, 1970). Cuticles with crenulated cells are almost absent suggesting predominance of sun leaves; consistent through the sequence (Barclay, 2011).
Plant age (juvenile vs. adult)	Donovan and Ehleringer (1992)	Mature trees are the overwhelming source for leaves in plant litter (Burnham, 1994); leaves in the Dakota Fm. were probably sun leaves from angiosperm trees (Barclay et al., 2010).
Growth form and deciduousness	Smedley et al. (1991); Donovan and Ehleringer (1992); Brooks et al. (1997)	Deciduousness is typically manifested as mats of leaves from only one species (Gastaldo and Staub, 1999); plant assemblages in the Dakota Fm. always contained a mixture of species. Changes in C/N ratios (Fig. S2) might be related to deciduousness; however, covariance with stomatal index suggests predominant pCO_2 control on C/N ratios.
Nutrient deficiency	Toft et al. (1989)	Deficiency unlikely: generally high weathering rates; potential nutrient redistribution by increased fire frequency in "–a2" (Baker et al., 2019). Changes in C/N ratios (Fig. S2) might be related to nutrient availability; however, covariance with stomatal index suggests predominant pCO_2 control on C/N.
pCO_2 change	Schubert and Jahren (2012); Porter et al. (2017); Hare et al. (2018)	Fractionation response to pCO_2 change might have enhanced the primary isotopic response of plant tissue to a $\delta^{13}C$ change of the atmospheric reservoir.

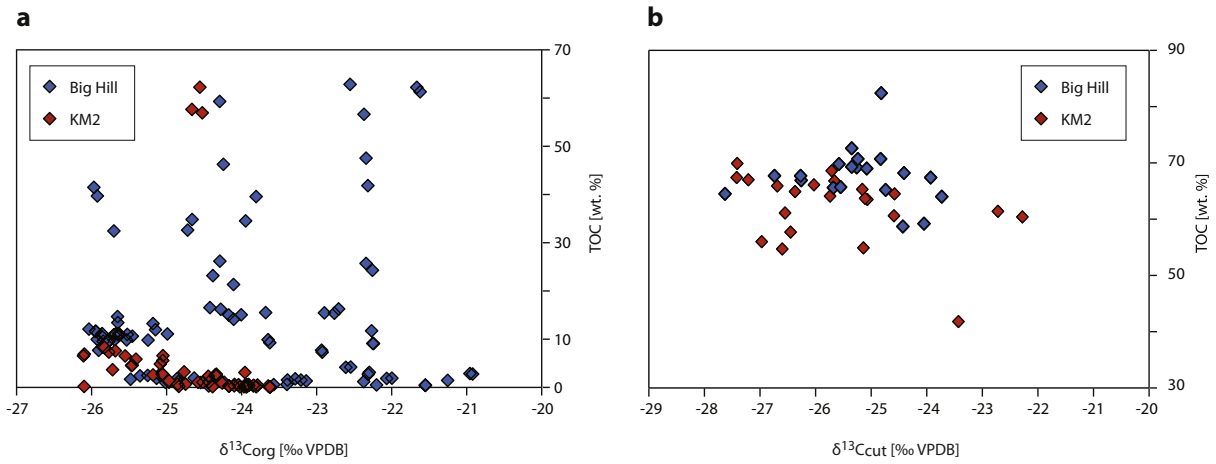

Fig. 9. Scatter plots of $\delta^{13}C_{org}$ (a) and $\delta^{13}C_{cut}$ (b) vs. total organic carbon for the Big Hill and KM2 sections.

condensation between sequences S3 and S4 could be responsible for the poor resolution of "phase B".

An explanation of the basinward loss of excursions "–a2" and "–a3" is more complex. Since local conditions and landward influx of marine organic carbon have been excluded as the principal control on the isotopic excursions (Section 5.1), the basinward loss should be attributed to (1) preservational bias in the marine record due to transgressive condensation and biogenic mixing, (2) differential response of the atmospheric and oceanic reservoirs to carbon emissions, or (3) differences in the isotopic fractionation in marine plankton vs. higher plants.

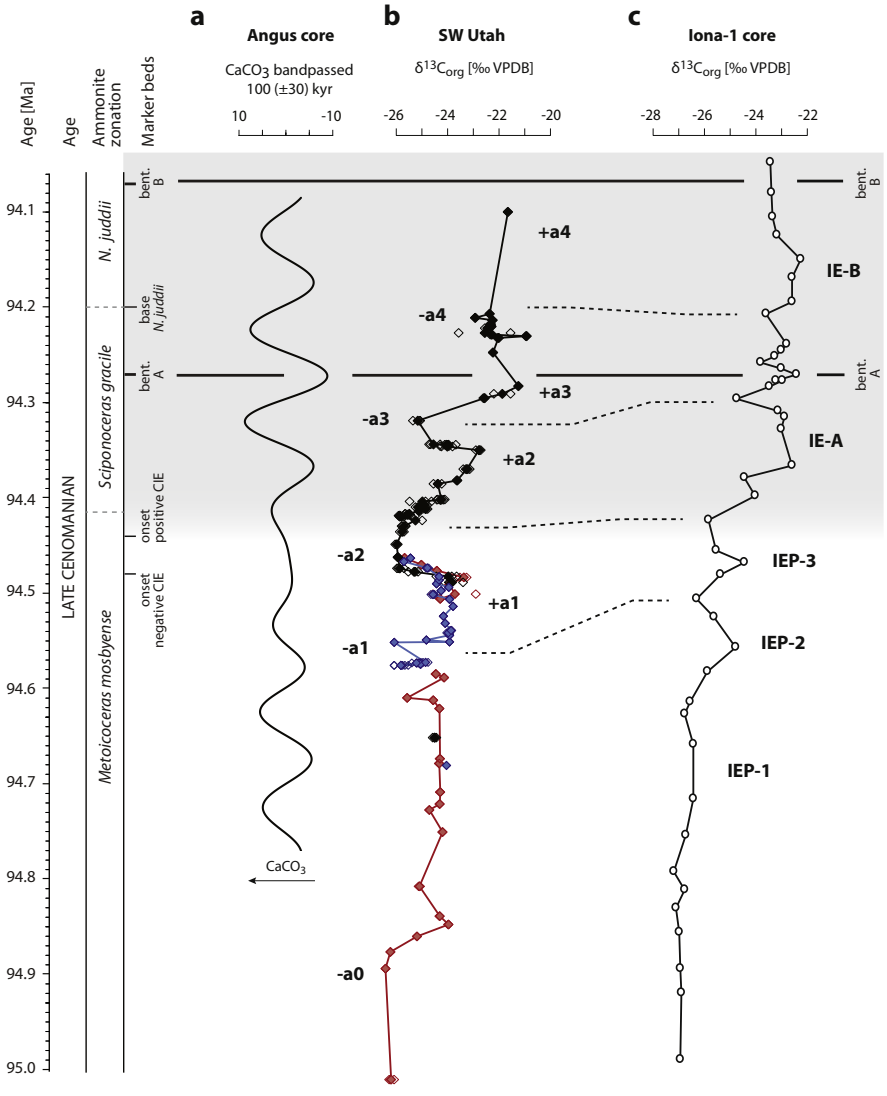

Fig. 10. Eccentricity-scale structure of $\delta^{13}C_{org}$ variations in SW Utah (this study) and Iona-1 core, Texas (Eldrett et al., 2014). (a) Filtered ~100 kyr eccentricity signature from the Angus core $CaCO_3$ record (Ma et al., 2014). CIE = carbon-isotope excursion of OAE2. (b) Time-domain $\delta^{13}C_{org}$, SW Utah. Symbols as in Fig. 8. (c) Time-domain $\delta^{13}C_{org}$, Iona-1 (floating age model from Eldrett et al., 2014; note that numerical age calibration in Eldrett et al., 2014, differs from the age calibration employed in this study; floating age model is therefore preferred for this comparison). Medium-term $\delta^{13}C$ excursions are labeled and their possible relationships to $\delta^{13}C$ changes in the Iona core are indicated.

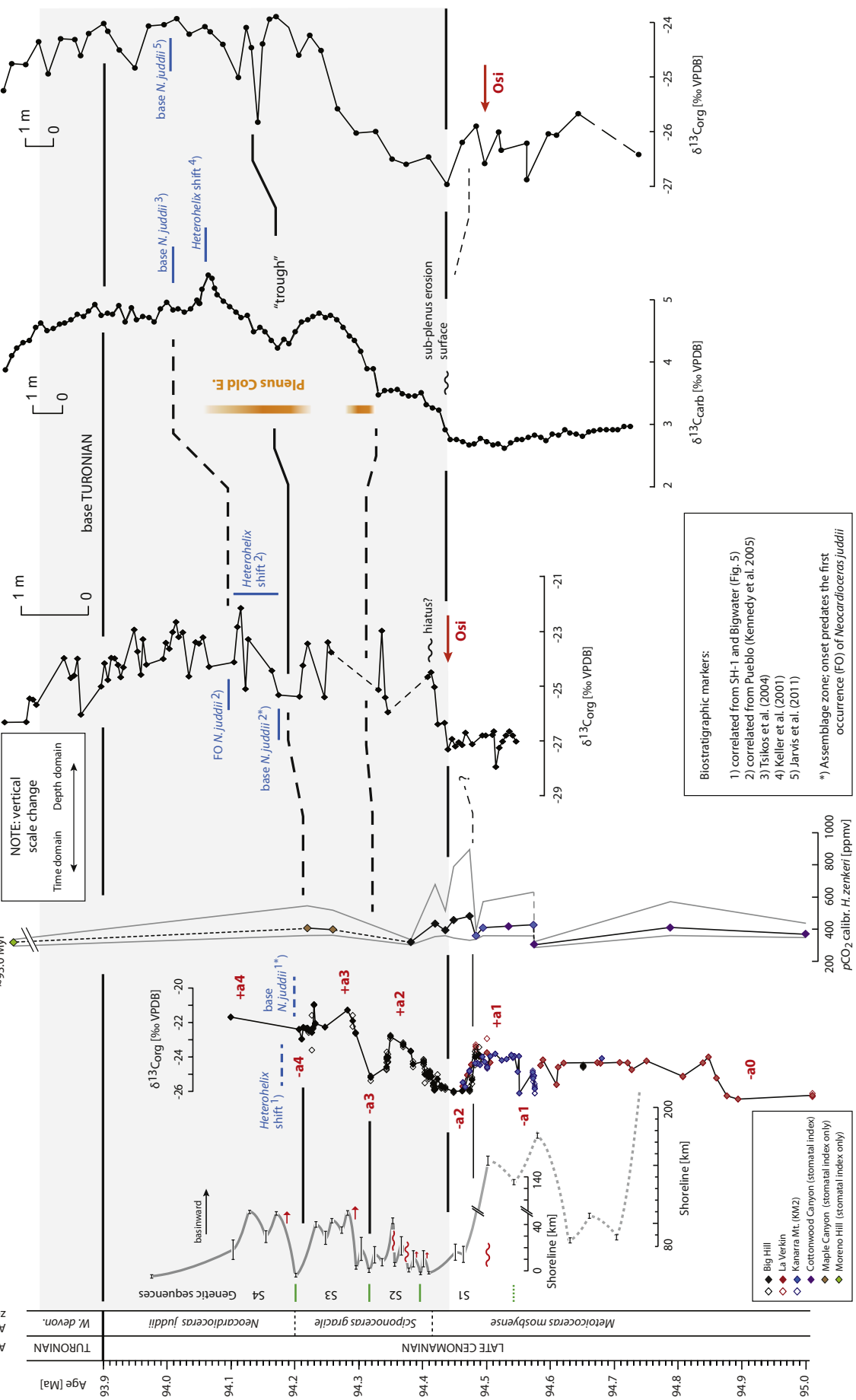

Fig. 11. Correlation to European sections. (a) Transgressive-regressive history, $\delta^{13}C_{org}$ and calibrated estimates of pCO_2 from stomatal-index data (modified after Barclay et al., 2010), SW Utah, plotted in the time domain. The calibration to atmospheric pCO_2 is based on herbarium training data set of *Hypodaphnis zenkeri* (for details see Barclay et al., 2010). Grey margins delineate the 95% confidence interval. (b) USGS #1 Portland core $\delta^{13}C_{org}$ data plotted in the depth domain (after Sageman et al., 2006). *) *N. juddii* Zone has been delineated as an assemblage zone, in the Western Interior Basin; its onset predates the first appearance of the ammonite *Neocardioceras juddii* (Elder, 1991; Elder et al., 1994; Kennedy et al., 2005). (c) Eastbourne $\delta^{13}C_{carb}$ data plotted in the depth domain (after Tsikos et al., 2004). Timing of the Plenus Cold Event and its prelude (orange bars) is adopted from Jenkyns et al. (2017). (d) Pont d'Issole $\delta^{13}C_{org}$ data plotted in the depth domain (after Jarvis et al., 2011).

Preservational bias appears particularly relevant for the negative excursions "–a2" and "–a3", because they are relatively brief and coincide with intervals of siliciclastic starvation. In spite of enhanced carbonate production, bulk sedimentation rates remain low in hemipelagic and pelagic sites, thus making any short-term signal prone to distortion by biogenic mixing. For example, considering sedimentation rates on the order of 0.5 to 1.0 cm/kyr (Bridge Creek Limestone; Meyers et al., 2001), intense mixing in the uppermost 5–10 cm of the sediment column, and heterogeneous mixing to the depth of 20–35 cm (cf. Savrda, 1998), any shift in isotopic signature on time scales shorter than 20 kyr would be smoothed. Physical reworking is another factor to consider in hemipelagic sites (e.g., Bridge Creek Limestone; Meyers and Sageman, 2004; Du Vivier et al., 2014; Eldrett et al., 2014). A possible argument for depositional bias in some of the marine records comes from the preservation of negative anomalies in weakly bioturbated strata of Tarfaya (Kuhnt et al., 2017) and a relatively high-accommodation carbonate-platform setting in Mexico (Elrick et al., 2009).

The negative excursions could theoretically represent a non-steady state response of the atmospheric reservoir to subaerial carbon emissions. In such a scenario, the absence of an oceanic record would be related to dilution of the atmospheric signature in the larger oceanic inventory. Such a differential response is, however, limited to very short-term (centennial to millennial) perturbations. On the 10-kyr time scales interpreted for the negative excursions, atmospheric chemistry can be expected to equilibrate with the ocean (e.g., Zeebe, 2012).

The last option to consider is a sensitivity of carbon-isotope fractionation to changes in the atmospheric concentration of CO_2. As noted earlier, the $\delta^{13}C_{org}$ signature probably involves a component related to the physiological response of plants to changing pCO_2. A higher sensitivity of the isotopic discrimination in terrestrial plants relative to marine plankton could explain pronounced negative excursions in the terrestrial organics (cf. Franks et al., 2014). Although the veracity of fractionation relationships related to pCO_2 levels is still debated, the above scenario appears consistent with isotopic signatures from fossil wood (Takashima et al., 2010) that exhibit negative anomalies in the OAE2 interval. We conclude that the preservation of negative anomalies in the marginal-marine record is probably related to better temporal resolution in the coastal transgressive facies and/or enhanced sensitivity of terrestrial plants to pCO_2.

5.4. Volcanogenic signature in $\delta^{13}C$

The negative excursions "–a1", "–a2" and "–a3" overlap with the interval of a major volcanic pulse documented in osmium isotopes (Turgeon and Creaser, 2008; Du Vivier et al., 2014), and can be considered a possible record of volcanogenic CO_2 emissions from the Caribbean or Arctic large igneous provinces. To explain the magnitude of these anomalies with volcanogenic carbon, which is isotopically close to the mean $\delta^{13}C$ of the ocean-atmosphere reservoir (Kump and Arthur, 1999), the perturbation would have to involve repeated emissions of 28,000 to 43,000 Pg of carbon, each lasting 10–20 kyr and representing over 60 to 90% of the global exogenic carbon inventory (Table S3). The volumes and rates could be substantially smaller if the isotopic shift was assisted by a CO_2-controlled change in fractionation (Porter et al., 2017). However, additional features that are difficult to reconcile with a volcanogenic origin include (1) the coordination of intervening positive excursions "+a1", "+a2" and "+a3" with relative sea-level falls (Figs. 4 and 8), and (2) the recurrence interval, which resembles astronomical pacing.

Eustatic sea-level rise is an expected product of submarine volcanism. It can be partly compensated by subsequent magma cooling, but this process is slow and unlikely to develop eustatic fall whose rate would exceed the rate of foredeep subsidence. The indices for relative sea-level falls (Laurin and Sageman, 2007) and close coordination between sea-level oscillations and $\delta^{13}C$ variability thus argue against a volcanogenic origin for the negative anomalies. In addition, the carbon-isotope shifts recur on time scales that closely resemble astronomical pacing of organic-carbon burial in the monsoonal belt immediately prior to OAE2 (Mitchell et al., 2008; Lanci et al., 2010; Laurin et al., 2016). The carbon-isotope ratio in organic carbon makes it a (~5 times) more efficient mechanism for developing $\delta^{13}C$ anomalies. A previously documented coincidence of the osmium-isotope shift with a 405-kyr maximum in seasonality modulation (Laurin et al., 2016) is another aspect to consider. Hence, although some volcanogenic signature should be present in the study interval, it is probably masked by a stronger, climate-controlled variability in $\delta^{13}C$.

5.5. Astronomical pacing of $\delta^{13}C$

The recurrence interval of negative excursions "–a1" through "–a4" ranges from 80 to 120 kyr (Fig. 8), resembling the periods of short eccentricity (95–124 kyr; Laskar et al., 2004). The study interval is too short to provide robust statistical arguments, but coeval marine strata in the SH-1 core bear a strong eccentricity signature (Jones et al., 2019), and a comparable record of eccentricity-paced $\delta^{13}C$ anomalies was identified in the Iona core (Eldrett et al., 2014; Fig. 10). Notably, the eccentricity-like structure of carbon-isotope anomalies forms a consistent follow-up of a prominent, eccentricity-paced cyclicity of the pre-OAE2 interval (Mitchell et al., 2008; Lanci et al., 2010; Ma et al., 2014; Wendler et al., 2014). Previous studies (Laurin et al., 2016; Batenburg et al., 2016) have shown that the onset of OAE2 overlaps with a 405-kyr eccentricity maximum. If so, then the initial phase of OAE2 should be characterized by relatively high amplitudes of eccentricity (and precessional index). With the buildup of OAE2, eccentricity amplitudes decline (Laurin et al., 2016), paralleled by an increase in obliquity variance in marine proxies of carbon burial (e.g., Meyers et al., 2012b; Charbonnier et al., 2018). The observed pattern in $\delta^{13}C$ is therefore compatible with previous results on astronomical control in this interval.

Orbital eccentricity controls the amplitude of precession-paced changes in seasonal insolation at most latitudes (e.g., Berger et al., 1993; Laskar et al., 1993). The type and location of carbon reservoirs responsible for the $\delta^{13}C$ variability cannot be determined at present, but terrestrial carbon reservoirs (e.g., lakes, soil, peat) in the monsoonal belt could provide both sufficient volumes and sensitivity to insolation on the precessional and eccentricity time scales (e.g., Rossignol-Strick, 1983; Flögel et al., 2008). It also offers an explanation of the observed correlation between $\delta^{13}C$ changes and sea-level, as discussed below.

5.6. Carbon cycle and sea-level change

The negative carbon-isotope excursions are associated with brief intervals during medium-term transgressive phases (Figs. 4 and 8). If sediment supply and tectonics are excluded as a control on medium-term shoreline movements in the study interval (see discussion in Laurin and Sageman, 2007, and Text S5), then the data suggest a coordination of negative $\delta^{13}C$ shifts in the atmospheric carbon reservoir and increments in eustatic rise (superimposed upon a long-term accommodation driven by tectono-eustasy and foreland subsidence). Conversely, medium-term enrichment in ^{13}C is preferred during intervals when the rates of sea-level rise are reduced, or the sea level falls. Such coordination can provide important insights into the climate mechanisms.

Relative sea-level falls documented in the study interval can be attributed to eustatic falls, the magnitudes of which exceeded 2 m, but remained safely below 12 m (Text S6). Mechanisms capable of producing such fluctuations on the precessional and eccentricity time scales involve (i) thermal contraction of seawater, (ii) glacioeustasy, and (iii) aquifer eustasy (see review in Sames et al., 2016).

The first mechanism to consider is thermal contraction of seawater (e.g., Schulz and Schäfer-Neth, 1997). An early phase of OAE II was accompanied by a transient cooling of the Atlantic surface water

(Forster et al., 2007; Sinninghe Damsté et al., 2010). At mid latitudes the surface temperature might have dropped by up to 12 °C, with short-term cooling rates of the surface water reaching a maximum of 3.5–7 °C in 10 kyr (Sinninghe Damsté et al., 2010). Depending on ocean overturning rates these changes might have been sufficient to generate small-scale changes in sea level by thermal contraction. However, it would require an extreme scenario, such as cooling of the entire ocean by an average of 3 °C in 10 kyr (assuming mean expansion coefficient of $3.2 \times 10^{-4} K^{-1}$) to reach the rate of long-term accommodation estimated for the study interval. Such a rate of ocean-wide temperature change would be comparable to the rate of ocean cooling during Pleistocene glacial transitions; the greenhouse world with its low latitudinal temperature gradients, slow ocean overturning rates and a lack of sea ice is unlikely to support cooling of this rate and magnitude. In addition, the cooling of Atlantic surface temperatures documented by Forster et al. (2007) and Sinninghe Damsté et al. (2010) probably correlates with the Plenus Cold event, and therefore postdates sequences S1 and S2 in Utah (Fig. S3).

The second possibility - glacioeustasy - can be expected to act in tandem with permafrost storage of methane clathrates, potentially leading to a coordination between sea-level change and $\delta^{13}C$ similar to that observed in southwestern Utah. Although controversial for the peak Cretaceous greenhouse, glacioeustasy could be facilitated by a transient drop in pCO_2 and favorable orbital configurations (cf. Flögel et al., 2011a). However, inter-annual ice accumulation would likely be short-lived, tied to episodes of low obliquity and precession-paced aphelial summers. The rhythm would be dominated by the ~40-kyr obliquity cycle (cf. Huybers, 2006). Eccentricity-scale glaciation would be possible only at low eccentricity and would require very low pCO_2 to cross the glaciation threshold. If CO_2 sequestration during OAE2 (Arthur et al., 1988) provided the background for glacial accumulation, then glacioeustatic sea-level falls would likely coincide with cooling episodes such as the Plenus Cold Event (Gale and Christensen, 1996; review in Jenkyns et al., 2017). Correlation to European sections, however, suggests that the Plenus Cold Event and its prelude are centered at major transgressive intervals separating medium-term genetic sequences in SW Utah (Fig. 11). In both cases, the cooling was already in retreat at the onset of possible forced regression. Such a context is incompatible with glacioeustatic forcing of the genetic sequences. Finally, application of the glacioeustatic hypothesis to the study interval would require lowered pCO_2 prior to the major phase of OAE2 carbon sequestration (see indices of sea-level fall in sequence S1; Laurin and Sageman, 2007). The available data (Barclay et al., 2010) do not support such a possibility.

Considering the above limitations, aquifer eustasy (Hay and Leslie, 1990; Jacobs and Sahagian, 1993; Wendler et al., 2014, 2016; Wagreich et al., 2014) offers the most straightforward explanation, consistent with both the greenhouse conditions and the eccentricity rhythm. According to a compilation presented by Sames et al. (2016), the maximum capacity of aquifer eustasy (over 10 m of sea-level change) occurs at or below the precessional time scales. Variations in the past monsoonal lake levels (e.g., Triassic Newark basin; Olsen and Kent, 1999) further suggest that asymmetry in the rates of aquifer recharge and discharge provides a viable mechanism for amplifying the eccentricity component in a primarily precession-paced system. The potential relationship between sea-level change and $\delta^{13}C$ excursions is illustrated with a simple conceptual model, in which positive precipitation-evaporation balance related to strong summer monsoons supports aquifer charge, terrestrial biomass production and carbon burial (positive $\delta^{13}C$ shift, interfering positively with the background OAE2 anomaly). In contrast, net aquifer discharge during weak monsoonal configurations is accompanied by reduced terrestrial carbon burial and accelerated carbon remineralization (negative $\delta^{13}C$ shift; cf. Briggs et al., 2007; Fig. 12). The highest rates of both eustatic sea-level rise and influx of ^{13}C-depleted carbon into the ocean-atmosphere system are favored during aphelial (dry) summers following high eccentricity ($e > |th1|$; Fig. 12). In this scenario, the lag of the negative $\delta^{13}C$ anomaly behind the onset of sea-level rise is partly related to a lag between the onset of lake desiccation (net transfer of water to the ocean) and exposure of organic deposits at the lake bottom (analogous to the lag observed in Pleistocene eolian input to the equatorial Atlantic; Pokras and Mix, 1987). The inherent response time of the carbon cycle likely contributed to the lagged $\delta^{13}C$ signature in negative anomalies (cf. Zeebe et al., 2017; Laurin et al., 2017), whereas interference with the background OAE2 signature (see also Section 5.7) might be responsible for the early onset of the positive anomaly "+a2" relative to sequence S2 (Fig. 8).

Given the mid-latitude position (~40°N) and limited land area of the western margin of the WIS, the study site was probably external to the hypothesized aquifer "factory" (which might have been located in Asia, Africa or South America). However, the northern margin of the subtropical high-pressure system was situated immediately south of the study area (Chumakov et al., 1995) suggesting that seasonal-insolation changes similar to those involved in the hypothesized aquifer eustasy might be inscribed in the local climate. In this context, the increase in fire frequency during the negative isotope anomaly "–a2" documented by Baker et al. (2019, in press) can be viewed as an argument in support of the conceptual model.

5.7. Temporal scaling of causal mechanisms

The relative phasing of medium-term (~100-kyr) sea-level change and carbon-isotope excursions discussed in this paper contrasts with the phase relationships interpreted for longer (≥400 kyr) time scales (e.g., Jarvis et al., 2006; Wendler et al., 2014). Hence, the coupling between carbon burial and aquifer charge inferred here appears limited to relatively short time intervals. A possible explanation lies in the limited storage capacity of shallow aquifers (including lakes and rivers) that can affect carbon production and burial. While these aquifer levels fluctuate on relatively short time scales, the longer-term aspect of aquifer eustasy may require involvement of deeper groundwater levels that are not coupled directly to the exogenic carbon cycle.

The coordination between negative isotope anomalies and sea-level rises observed on the astronomical time scale also contrasts with the long-term pattern, in which the ^{13}C-enriched signature of OAE 2 correlates with a major (tectono-eustatic) sea-level rise (e.g., Schlanger and Jenkyns, 1976). The seeming incompatibility originates from differences in the nature of the background OAE2 conditions, which are induced by submarine volcanism (e.g., Snow et al., 2005; Turgeon and Creaser, 2008), and the superimposed, insolation-controlled variability in the hydrological system. These processes are unrelated, but together constitute the paleoclimate signature of OAE2.

6. Conclusions

1) Terrestrial and marginal-marine records of OAE2 in southwestern Utah preserve information on changing volume and carbon-isotope composition of the atmospheric CO_2 inventory.
2) ~100-kyr excursions in $\delta^{13}C_{org}$ characterize the initial phase of OAE2. They originate from a combination of $\delta^{13}C$ changes in the atmospheric reservoir and physiological response of higher plants to changing pCO_2. These excursions are absent or muted in the open-marine record due to preservational bias and/or differences in isotopic fractionation between terrestrial plants and marine plankton. The terrestrial record thus provides new details on the structure of carbon-cycle perturbations during OAE2.
3) During the initial phase of OAE2, prior to the peak carbon burial and strengthening of the obliquity control, the carbon-cycle perturbations were dictated by insolation changes with a prominent eccentricity component.
4) Negative excursions in the terrestrial-sourced $\delta^{13}C_{org}$ are coordinated with accelerations in sea-level rise, while medium-term

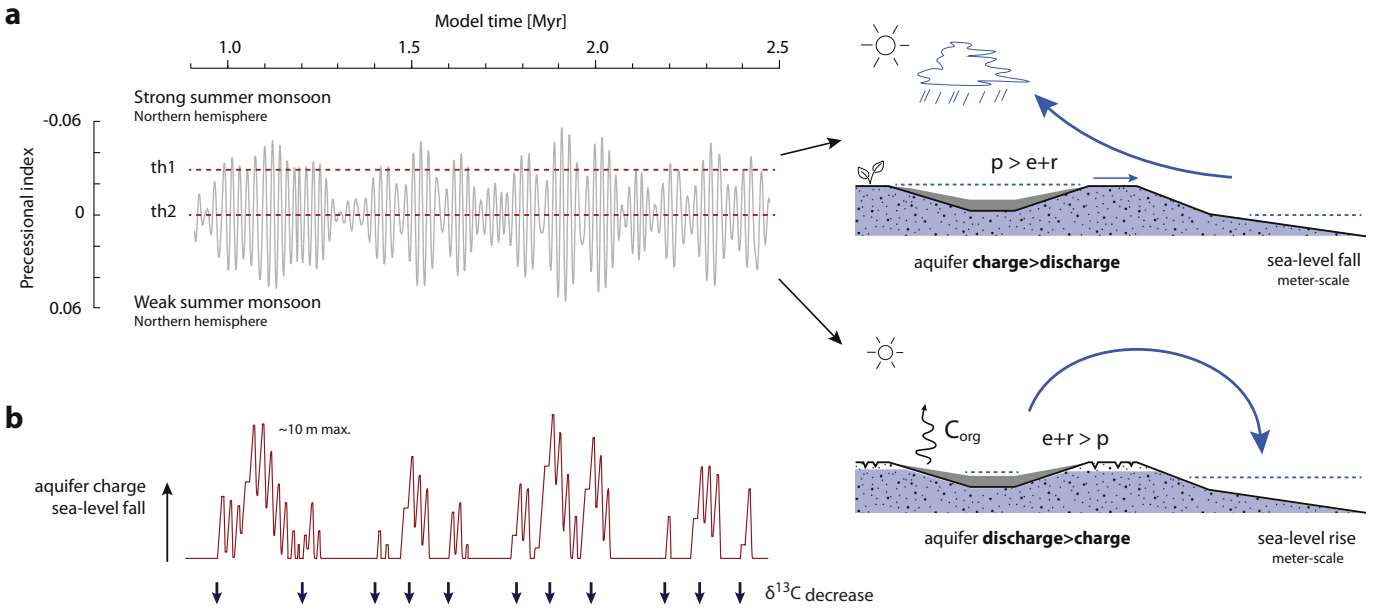

Fig. 12. Conceptual model of the hypothesized relationships between insolation-controlled aquifer charge/discharge, meter-scale sea-level change and carbon storage in the monsoonal belt. (a) Precessional forcing; th1 and th2 are thresholds for aquifer charge and discharge, respectively. For details see supplementary Text S4. (b) Fluctuations in net aquifer charge controlled by the precessional index. Black arrows denote the first aphelial (i.e., dry) summers following the maximum lake level at the eccentricity scale; these intervals are considered to have the highest potential for rapid subaerial degradation of organic carbon from the terrestrial reservoir. The release of ^{13}C-depleted carbon can be facilitated by increased wildfire frequency (cf. Finkelstein et al., 2006; Baker et al., 2019, in press). This scenario produces negative δ^{13}C excursions penecontemporaneous with the maximum rate of net water transfer to the ocean (eustatic sea-level rise), similar to the timing observed in the Dakota Formation. Explanation: p = precipitation, e = evaporation, r = surface runoff.

intervals of ^{13}C enrichment overlap with regressions and evidence for relative sea-level fall. These relationships can be explained by changes in aquifer charge accompanied by biomass burial/degradation in the monsoonal belt.

5) Further understanding of the paleoclimate signature of OAE2 may require consideration of both oceanic and terrestrial contributions to the Late Cenomanian hydrological regime and carbon cycle.

Acknowledgements

The Czech Science Foundation (project 17-10982S) supported the research efforts of J. Laurin. Initial collection of samples by R. Barclay was funded by a NSF grant (EAR-0643290) to B. Sageman and J. McElwain. The Peter Buck Foundation supported R. Barclay while in the Paleobiology Department at the Smithsonian's National Museum of Natural History. The Field Museum in Chicago, Illinois is thanked for housing and curating the plant cuticle and rock samples that were the foundation of this study. Rock samples were processed under the direction of Petra Sheaffova at Northwestern University by undergraduate students Colin Carney, Peter McVary, and Jackie Beard. Carbon isotope samples were run by staff in the Department of Earth & Planetary Sciences at Northwestern University. The manuscript benefited greatly from the comments of two anonymous reviewers.

Data availability

Carbon-isotope, stomatal-index, *n*-alkane and U-Pb data discussed in this paper are included in the Mendeley Data repository.

Appendix A. Supplementary data

Supplementary data to this article can be found online at https://doi.org/10.1016/j.palaeo.2019.03.019.

References

Adams, D., Hurtgen, M., Sageman, B., 2010. Volcanic activation of biogeochemical cascade regulates oceanic anoxic event 2. Nat. Geosci. 201–204.
Arens, N.C., Jahren, A.H., Amundson, R., 2000. Can C3 plants faithfully record the carbon isotopic composition of atmospheric carbon dioxide? Paleobiology 26, 137–164.
Arthur, M.A., Dean, W.E., Pratt, L.M., 1988. Geochemical and climatic effects of increased marine organic carbon burial at the Cenomanian/Turonian boundary. Nature 335, 714–717. https://doi.org/10.1038/335714a0.
Aucour, A.M., Gomez, B., Sheppard, S.M.F., Thevenard, F., 2008. δ^{13}C and stomatal number variability in the Cretaceous conifer *Frenelopsis*. Palaeogeogr. Palaeoclimatol. Palaeoecol. 257, 462–473.
Baker, S.J., Belcher, C.M., Barclay, R.S., Hesselbo, S.P., Laurin, J., Sageman, B.B., 2019. CO_2 Induced Climate Forcings on the Fire Record during Cretaceous OAE2. in press. (GSA Bulletin).
Barclay, R. S., 2011, Testing The Driving Mechanisms For Ocean Anoxic Event 2 (94Ma) Using pCO_2 Estimates And Carbon Isotopes Derived From Fossil Plant Material In The Dakota Formation Of Southwestern Utah. Ph.D. Dissertation. Northwestern University (Evanston, USA). 305 pp.
Barclay, R.S., McElwain, J.C., Sageman, B.B., 2010. Carbon sequestration activated by a volcanic CO_2 pulse during Ocean Anoxic Event 2. Nat. Geosci. 3, 205–208. https://doi.org/10.1038/ngeo757.
Barclay, R.S., Rioux, M., Meyer, L.B., Bowring, S.A., Johnson, K.R., Miller, I.M., 2015. High precision U/Pb zircon geochronology for Cenomanian Dakota Formation floras in Utah. Cretac. Res. 52, 213–237.
Barral, A., Lécuyer, C., Gomez, B., Fourel, F., Daviero-Gomez, V., 2015. Effects of chemical preparation protocols on δ13C values of plant fossil samples. Palaeogeogr. Palaeoclimatol. Palaeoecol. 438, 267–276.
Batenburg, S.J., De Vleeschouwer, D., Sprovieri, M., Hilgen, F.J., Gale, A.S., Singer, B.S., Koeberl, C., Coccioni, R., Claeys, P., Montanari, A., 2016. Orbital control on the timing of oceanic anoxia in the Late Cretaceous. Clim. Past Discuss. https://doi.org/10.5194/cp-2015-182.
Beerling, D.J., 1996. Ecophysiological responses of woody plants to past CO_2 concentrations. Tree Physiol. 16, 389–396.
Beerling, D.J., Fox, A., Stevenson, D.S., Valdes, P.J., 2011. Enhanced chemistry-climate feedbacks in past greenhouse worlds. Proc. Natl. Acad. Sci. U. S. A. 108, 9770–9775. https://doi.org/10.1073/pnas.1102409108.
Berger, A., Loutre, M.-F., Tricot, C., 1993. Insolation and Earth's orbital periods. J. Geophys. Res. 98 (D6), 10,341–10,362. https://doi.org/10.1029/93JD00222.
Berner, R.A., 2006. GEOCARBSULF: a combined model for Phanerozoic atmospheric O_2 and CO_2. Geochim. Cosmochim. Acta 70, 5653–5664. https://doi.org/10.1016/j.gca.2005.11.032.
Blättler, C.L., Jenkyns, H.C., Reynard, L.M., Henderson, G.M., 2011. Significant increases in global weathering during Oceanic Anoxic Events 1a and 2 indicated by calcium isotopes. Earth Planet. Sci. Lett. 309, 77–88.

Bray, E.E., Evans, E.D., 1961. Distribution of n-Paraffins as a. Clue to Recognition of Source Beds: Geochimica Et Cosmochimica Acta 22 (1), 2–15.
Briggs, J., David J. Large, Colin Snape, Trevor Drage, David Whittles, Mick Cooper, Joe H. S. Macquaker, Baruch F. Spiro, 2007, Influence of climate and hydrology on carbon in an early Miocene peatland. Earth and Planetary Science Letters, Volume 253, Issues 3–4, 30 January 2007, Pages 445–454.
Brooks, J.R., Flanagan, L.B., Buchmann, N., Ehleringer, J.R., 1997. Carbon isotope composition of boreal plants: functional grouping of life forms. Oecologia 110, 301–311.
Burnham, R.J., 1994. Patterns in tropical leaf litter and implications for angiosperm paleobotany. Rev. Palaeobot. Palynol. 81, 99–113.
Bush, R.T., McInerney, F.A., 2013. Leaf wax n-alkane distributions in and across modern plants. Implications for paleoecology and chemotaxonomy: Geochimica et Cosmochimica Acta 117, 161–179.
Bush, R.T., Wallace, J., Currano, E.D., Jacobs, B.F., McInerney, F.A., Dunn, R.E., Tabor, N. J., 2017. Cell anatomy and leaf $\delta^{13}C$ as proxies for shading and canopy structure in a Miocene forest from Ethiopia. Palaeogeography, Palaeoclimatology, Palaeoecology 485(Supplement C): 593-604.
Carpenter, K., 2014. Where the sea meets the land—the unresolved Dakota problem in Utah, in MacLean, J.S., Biek, R.F., and Huntoon, J.E., editors. Geology of Utah's Far South: Utah Geological Association Publication 43, 357–372.
Cernusak, L.A., Ubierna, N., Winter, K., Holtum, J.A.M., Marshall, J.D., Farquhar, G.D., 2013. Environmental and physiological determinants of carbon isotope discrimination in terrestrial plants. New Phytol. 200, 950–965.
Charbonnier, G., Boulila, S., Spangenberg, J.E., Adatte, T., Föllmi, K.B., Laskar, J., 2018. Obliquity pacing of the hydrological cycle during the Oceanic Anoxic Event 2. Earth Planet. Sci. Lett. 499, 266–277.
Chumakov, N.M., Zharkov, M.A., Herman, A.B., Doludenko, M.P., Kalandadze, N.N., Lebedev, E.A., Ponomarenko, A.G., Rautian, A.S., 1995. Climate belts of the Mid-cretaceous time. Stratigr. Geol. Correl. 3, 241–260.
Clark, R.J., Blumer, M., 1967. Distribution of n-paraffins in marine organisms and sediment. Limnol. Oceanogr. 12, 79–87.
Dean, W.E., Arthur, M.A., Claypool, G.E., 1986. Depletion of ^{13}C in Cretaceous marine organic matter: source, diagenetic or environmental signal? Mar. Geol. 70, 119–157. https://doi.org/10.1016/0025-3227(86)90092-7.
Donovan, L.A., Ehleringer, J.R., 1992. Contrasting water-use patterns among size and life-history classes of a semiarid shrub. Funct. Ecol. 6, 482–488.
Du Vivier, A.D.C., Selby, D., Sageman, B.B., Jarvis, I., Gröcke, D.R., Voigt, S., 2014. Marine $^{187}Os/^{188}Os$ isotope stratigraphy reveals the interaction of volcanism and ocean circulation during Oceanic Anoxic Event 2. Earth Planet. Sci. Lett. 389, 23–33. https://doi.org/10.1016/j.epsl.2013.12.024.
Ehleringer, J.R., Field, C.B., Lin, Z.F., Kuo, C.Y., 1986. Leaf carbon isotope and mineral-composition in subtropical plants along an irradiance cline. Oecologia 70, 520–526.
Elder, W.P., 1989. Molluscan extinction patterns across the. Cenomanian-Turonian Stage boundary in the Western Interior of the United States: Paleobiology 15 (3), 299–320.
Elder, W.P., 1991. Molluscan paleoecology and sedimentation patterns of the Cenomanian–Turonian extinction interval in the southern Colorado Plateau region. In: Nations, J.D., Eaton, J.G. (Eds.), Stratigraphy. Depositional Environments, and Sedimentary Tectonics of the Western Margin, Cretaceous Western Interior Seaway: Geological Society of America, Special Paper, vol. 260. pp. 113–137.
Elder, W. P., and Kirkland, J. I., 1985, Stratigraphy and depositional environments of the Bridge Creek Limestone Member of the Greenhorn Limestone at Rock Canyon Anticline near Pueblo, Colorado, in Pratt, L. M., Kauffman, E. G., and Zelt, F. B., eds., Fine-Grained Deposits and Biofacies of the Cretaceous Western Interior Seaway: evidence of Cyclic Sedimentary Processes, SEPM Society for Sedimentary Geology.
Elder, W.P., Gustason, E.R., Sageman, B.B., 1994. Correlation of basinal carbonate cycles to nearshore parasequences in the Late Cretaceous Greenhorn seaway, Western Interior U.S.A. Geol. Soc. Am. Bull. 106 (7), 892–902.
Eldrett, J.S., Minisini, D., Bergman, S.C., 2014. Decoupling of the carbon cycle during Ocean Anoxic Event-2. Geology v. 42, 567e570. https://doi.org/10.1130/G35520.1 no. 7.
Elrick, M., Molina-Garza, R., Duncan, R., Snow, L., 2009. C-isotope stratigraphy and paleoenvironmental changes across OAE2 (mid-Cretaceous) from shallow-water platform carbonates of southern Mexico. Earth Planet. Sci. Lett. 277, 295–306.
Farquhar, G.D., O'Leary, M.H., Berry, J.A., 1982. On the relationship between carbon isotope discrimination and the intercellular carbon dioxide concentration in leaves. Aust. J. Plant Physiol. 9, 121–137.
Finkelstein, D.B., Pratt, L.M., Brassell, S.C., 2006. Can biomass burning produce a globally significant carbon-isotope excursion in the sedimentary record? Earth Planet. Sci. Lett. 250, 501–510.
Flögel, S., Beckmann, B., Hofmann, P., Bornemann, A., Westerhold, T., Norris, R.D., Dullo, C., Wagner, T., 2008. Evolution of tropical watersheds and continental hydrology during the Late Cretaceous greenhouse; impact on marine carbon burial and possible implications for the future. Earth Planet. Sci. Lett. 274, 1–13.
Flögel, S., Wallmann, K., Kuhnt, W., 2011a. Cool episodes in the Cretaceous - exploring the effects of physical forcings on Antarctic snow accumulation. Earth Planet. Sci. Lett. 307, 279–288.
Flögel, S., Wallmann, K., Poulsen, C.J., Zhou, J., Oschlies, A., Voigt, S., Kuhnt, W., 2011b. Simulating the biogeochemical effects of volcanic CO_2 degassing on the oxygen-state of the deep ocean during the Cenomanian/Turonian Anoxic Event (OAE2). Earth Planet. Sci. Lett. 305, 371–384. 10.1016/j.epsl.2011.03.018.
Forster, A., Schouten, S., Moriya, K., Wilson, P.A., Sinninghe Damsté, J.S., 2007. Tropical warming and intermittent cooling during the Cenomanian/Turonian oceanic anoxic event 2: sea surface temperature records from the equatorial Atlantic. Paleoceanography 22, PA1219. https://doi.org/10.1029/2006PA001349.
Franks, P.J., Royer, D.L., Beerling, D.J., Van de Water, P.K., Cantrill, D.J., Barbour, M.M., Berry, J.A., 2014. New constraints on atmospheric CO_2 concentration for the Phanerozoic. Geophys. Res. Lett. 41. https://doi.org/10.1002/2014GL060457.
Frijia, G., Parente, M., 2008. Strontium isotope stratigraphy in the upper Cenomanian shallow-water carbonates of the southern Apennines: short-term perturbations of marine $^{87}Sr/^{86}Sr$ during the oceanic anoxic event 2. Palaeogeogr. Palaeoclimatol. Palaeoecol. 261, 15–29.
Gale, A.S. and Christensen, W.K., 1996. Occurrence of the belemnite *Actinocamax plenus* in the Cenomanian of SE France and its significance. Bull. Geol. Soc. Denmark, 43, 68–77.
Gastaldo, R.A., Staub, J.R., 1999. A mechanism to explain the preservation of leaf litter lenses in coals derived from raised mires. Palaeogeogr. Palaeoclimatol. Palaeoecol. 149, 1–14.
Gröcke, D.R., 2002. The carbon isotope composition of ancient CO_2 based on higher plant organic matter, Philos. Trans. R. Soc. London, Ser. A 360, 633–658. https://doi.org/10.1098/rsta.2001.0965.
Guy, R.D., Reid, D.M., Krouse, H.R., 1980. Shifts in carbon isotope ratios of two C3 halophytes under natural and artificial conditions. Oecologia 44, 241–247.
Hare, V.J., Loftus, E., Jeffrey, A., Ramsey, C.B., 2018. Atmospheric CO_2 effect on stable carbon isotope composition of terrestrial fossil archives. Nat. Commun. 9, 252.
Hattin, D.E., 1985. Distribution and significance of widespread, time-parallel pelagic limestone beds in Greenhorn Limestone (Upper Cretaceous) of the central Great Plains and southern Rocky Mountains. In: Pratt, L.M., Kauffman, E.G., Zelt, F.B. (Eds.), Fine-Grained Deposits and Biofacies of the Cretaceous Western Interior Seaway: Evidence of Cyclic Sedimentary Processes: SEPM. Field Trip Guidebook, vol. 4. pp. 28–37.
Hay, W.W., Leslie, M.A., 1990. Could possible changes in global groundwater reservoir cause eustatic sea level fluctuations? In: Geophysics Study Committee, C.o.P.S., Mathematics and Resources, National Research Council (Eds.), Sea Level Change: Studies in Geophysics. The National Academy of Sciences, National Academy Press, Washington D.C., pp. 161–170.
Hayes, J.M., 1993. Factors controlling ^{13}C contents of sedimentary organic compounds: principles and evidence. Marine Geology, v. 113, 111–125.
Heimhofer, U., Wucherpfennig, N., Adatte, T., Schouten, S., Schneebeli-Hermann, E., Gardin, S., Keller, G., Kentsch, S., Kujau, A., 2018. Vegetation response to exceptional global warmth during Oceanic Anoxic Event 2. Nat. Commun. 9, 3832.
Hintze, L.F., 1980. Geologic Map of Utah, 1:500,000: Utah Geological and Mineral Survey.
Huybers, P.J., 2006. Early Pleistocene glacial cycles and the integrated summer insolation forcing. Science 313 (5786), 508–511.
Jacobs, D.K., Sahagian, D.L., 1993. Climate-induced fluctuations in sea level during non-glacial times. Nature 361, 710–712.
Jahren, A.H., Arens, N.C., Harbeson, S.A., 2008. Prediction of atmospheric $\delta^{13}CO_2$ using fossil plant tissues. Rev. Geophys. 46, 1–12.
Jarvis, I., Gale, A.S., Jenkyns, H.C., Pearce, M.A., 2006. Secular variation in late cretaceous carbon isotopes: a new $\delta^{13}C$ carbonate reference curve for the Cenomanian–Campanian (99.6–70.6 Ma). Geol. Mag. 143, 561–608.
Jarvis, I., Lignum, J.S., Gröcke, D.R., Jenkyns, H.C., Pearce, M.A., 2011. Black shale deposition, atmospheric CO_2 drawdown, and cooling during the Cenomanian-Turonian Oceanic Anoxic Event. Paleoceanography 26, PA3201. https://doi.org/10.1029/2010PA002081.
Jenkyns, H.C., Dickson, A.J., Ruhl, M., van den Boorn, S.H.J.M., 2017. Basalt–seawater interaction, the Plenus Cold Event, enhanced weathering and geochemical change: deconstructing Oceanic Anoxic Event 2 (Cenomanian–Turonian, Late Cretaceous). Sedimentology 64, 16–43. https://doi.org/10.1111/sed.12305.
Jones, M.M., Sageman, B.B., Oakes, R.L., Parker, A.L., Leckie, R.M., Bralower, T.J., Sepúlveda, J., Fortiz, V., 2019. Astronomical pacing of relative sea level during Oceanic Anoxic Event 2: preliminary studies of the expanded SH#1 Core. Utah. GSA Bulletin. https://doi.org/10.1130/B32057.1.
Joo, Y.J., Sageman, B.B., 2014. Cenomanian to Campanian carbon isotope chemostratigraphy from the Western Interior Basin, U.S.A. J. Sediment. Res. 84, 529–542. https://doi.org/10.2110/jsr.2014.38.
Kennedy, W.J., Walaszczyk, I., Cobban, W.A., 2005. The global boundary stratotype section and point for the base of the Turonian stage of the cretaceous: Pueblo, Colorado. USA: Episodes 28 (2), 93–104.
Kohn, M.J., 2016. Carbon isotope discrimination in C3 land plants is independent of natural variations in pCO_2. Geochem. Persp. Let. 2, 35–43.
Kuhnt, W., Holbourn, A.E., Beil, S., Aquit, M., Krawczyk, T., Flögel, S., Chellai, E.H., Jabour, H., 2017. Unraveling the onset of Cretaceous Oceanic Anoxic Event 2 in an extended sediment archive from the Tarfaya-Laayoune Basin. Morocco, Paleoceanography 32, 923–946. https://doi.org/10.1002/2017PA003146.
Kump, L.R., Arthur, M.A., 1999. Interpreting carbon–isotope excursions: carbonate and organic matter. Chem. Geol. 161, 181–198. https://doi.org/10.1016/S0009-2541(99)00086-8.
Lanci, L., Muttoni, G., Erba, E., 2010. Astronomical tuning of the Cenomanian Scaglia Bianca Formation at Furlo. Italy. Earth Planet. Sci. Lett. 292, 231–237. https://doi.org/10.1016/j.epsl.2010.01.041.
Laskar, J., Joutel, F., Boudin, F., 1993. Orbital, precessional, and insolation quantities for the Earth from 20 Myr to +10 Myr. Astron. Astrophys. 270, 522–533.
Laskar, J., Robutel, P., Joutel, F., Gastineau, M., Correia, A.C.M., Levrard, B., 2004. A long-term numerical solution for the insolation quantities of the Earth. Astron. Astrophys. 428, 261–285. https://doi.org/10.1051/0004-6361:20041335.
Laurin, J., Sageman, B.B., 2007. Cenomanian-Turonian coastal record in SW Utah, USA: Orbital-scale transgressive-regressive events during oceanic anoxic event II. J. Sediment. Res. 77 (9–10), 731–756.
Laurin, J., Meyers, S.R., Galeotti, S., Lanci, L., 2016. Frequency modulation reveals the phasing of orbital eccentricity during Cretaceous Oceanic Anoxic Event II and the

Eocene hyperthermals. Earth Planet. Sci. Lett. 442, 143–156. https://doi.org/10.1016/j. epsl.2016.02.047.
Laurin, J., Růžek, B., Giorgioni, M., 2017. Orbital signals in carbon isotopes: phase distortion as a signature of the carbon cycle. Paleoceanography 32, 1236–1255. https://doi.org/10.1002/2017PA003143.
Leckie, R. M., 1985, Foraminifera of the Cenomanian-Turonian Boundary Interval, Greenhorn Formation, Rock Canyon Anticline, Pueblo, Colorado, in Pratt, L. M., Kauffman, E. G., and Zelt, F. B., eds., Fine-Grained Deposits and Biofacies of the Cretaceous Western Interior Seaway: evidence of Cyclic Sedimentary Processes, SEPM Society for Sedimentary Geology.
Liu, H., Liu, W., 2016. *n*-Alkane distributions and concentrations in algae, submerged plants and terrestrial plants from the Qinghai-Tibetan Plateau. Org. Geochem. 99, 10–22.
Ma, C., Meyers, S.R., Sageman, B.B., Singer, B.S., Jicha, B.R., 2014. Testing the astronomical time scale for oceanic anoxic event 2, and its extension into Cenomanian strata of the Western Interior Basin (USA). Geol. Soc. Am. Bull. 126 (7–8), 974–989.
Marshall, J.D., Brookes, J.R., Lajtha, K., 2007. Sources of variation in the stable isotopic composition of plants. In: Michener, R., Lajtha, K. (Eds.), Stable Isotopes in Ecology and Environmental Sciences. Blackwell Publishing, Oxford, pp. 22–50.
Martin, J.T., Juniper, B.E., 1970. The Cuticles of Plants. St. Martin's Press, New York, 347 pp.
Marzi, R., Torkelson, B.E., Olson, R.K., 1993. A revised carbon preference index. Org. Geochem. 20 (8), 1303–1306.
Meyers, P.A., 1997. Organic geochemical proxies of paleoceanographic, paleolimnologic, and paleoclimatic processes. Org. Geochem. 27 (5–6), 213–250.
Meyers, S. R., and Sageman, B. B., 2004, Detection, quantification, and significance of hiatuses in pelagic and hemipelagic strata. Earth Planet. Sci. Lett., v. 224, p. 55–72.
Meyers, S.R., Sageman, B.B., Hinnov, L.A., 2001. Integrated quantitative stratigraphy of the Cenomanian–Turonian Bridge Creek Limestone Member using evolutive harmonic analysis and stratigraphic modeling. J. Sediment. Res. 71, 628–644.
Meyers, S.R., Siewert, S.E., Singer, B.S., Sageman, B.B., Condon, D.J., Obradovich, J.D., Jicha, B.R., Sawyer, D.A., 2012a. Intercalibration of radioisotopic and astrochronologic time scales for the Cenomanian–Turonian boundary interval, Western Interior Basin, USA. Geology 40, 7–10. https://doi.org/10.1130/G32261.1.
Meyers, S.R., Sageman, B.B., Arthur, M.A., 2012b. Obliquity forcing of organic matter accumulation during Oceanic Anoxic Event 2. Paleoceanography 27, PA3212. https://doi.org/10.1029/2012PA002286.
Mitchell, R.N., Bice, D.M., Montanari, A., Cleaveland, L.C., Christianson, K.T., Coccioni, R., Hinnov, L.A., 2008. Oceanic anoxic cycles? Orbital prelude to the Bonarelli Level (OAE 2). Earth Planet. Sci. Lett. 26, 1–16. 10.1016/j.epsl.2007.11.026.
O'Brien, C.L., Robinson, S.A., Pancost, R.D., Sinninghe Damsté, J.S., Schouten, S., Lunt, D.J., Alsenz, H., Bornemann, A., Bottini, C., Brassell, S.C., Farnsworth, A., Forster, A., Huber, B.T., Inglis, G.N., Jenkyns, H.C., Linnert, C., Littler, K., Markwick, P., McAnena, A., Mutterlose, J., Naafs, B.D.A., Püttmann, W., Sluijse, A., van Helmonde, N.A.G.M., Vellekoope, J., Wagner, T., Wrobel, N.E., 2017. Cretaceous sea-surface temperature evolution: Constraints from TEX86 and planktonic foraminiferal oxygen isotopes. Earth Sci. Rev. 172, 224–247.
Ogg, J.G., Hinnov, L.A., Huang, C., 2012. Cretaceous. In: Gradstein, F.M., Ogg, J.G., Schmitz, M.D., Ogg, G.M. (Eds.), The Geological Time Scale 2012. Elsevier, Amsterdam, pp. 793–853.
Olsen, P.E., Kent, D.V., 1999. Long-period Milankovitch cycles from the late Triassic and Early Jurassic of eastern North America and their implications for the calibration of the Early Mesozoic time−scale and the long−term behaviour of the planets. Phil. Trans. R. Soc. Lond. A 357, 1761–1786. https://doi.org/10.1098/rsta.1999.0400.
Paul, C.R.C., Lamolda, M.A., Mitchell, S.F., Vaziri, M.R., Gorostidi, A., Marshall, J.D., 1999. The Cenomanian–Turonian boundary at Eastbourne (Sussex, UK): a pro- posed European reference section. Palaeogeogr. Palaeoclimatol. Palaeoecol. 150, 83–121. https://doi.org/10.1016/S0031-0182(99)00009-7.
Picha, F., 1986. The influence of preexisting tectonic trends on geometries of the Sevier orogenic belt and its foreland in Utah. In: Peterson, J.A. (Ed.), Paleotectonics and Sedimentation in the Rocky Mountain Region. United States: American Association of Petroleum Geologists, Memoir, vol. 41. pp. 309–320.
Pogge von Strandmann, P.A.E., Jenkyns, H.C., Woodfine, R.G., 2013. Lithium isotope evidence for enhanced weathering during Oceanic Anoxic Event 2. Nat. Geosci. 6, 668–672. https://doi.org/10.1016/j.epsl.2015.09.052.
Pokras, E.M., Mix, A.C., 1987. Earth's precessional cycle and Quaternary climatic change in tropical Africa. Nature 326, 486–487.
Porter, A.S., Yiotis, C., Montañez, I.P., McElwain, J.C., 2017. Evolutionary differences in $\delta^{13}C$ detected between spore and seed bearing plants following exposure to a range of atmospheric O_2: CO_2 ratios; implications for paleoatmosphere reconstruction. Geochim. Cosmochim. Acta 213 (p), 517–533.
Pratt, L.M., 1985, Isotopic studies of organic matter and carbonate in rocks of the Greenhorn Marine Cycle, in Pratt, L.M., et al., eds., Fine-grained de- posits and biofacies of the Cretaceous Western Interior Seaway: evidence of cyclic sedimentary processes: SEPM Field Trip Guidebook no. 4, p. 38–48.
Rieley, G., Collier, R.J., Jones, D.M., Eglinton, G., Eakin, P.A., Fallick, A.E., 1991. Sources of. Sedimentary Lipids Deduced from Stable Carbon Isotope Analyses of Individual Compounds: Nature 352 (6334), 425–427.
Rossignol-Strick, M., 1983. African monsoons, an immediate climate response to orbital insolation. Nature 304, 46–49.
Sageman, B.B., Meyers, S.R., Arthur, M.A., 2006. Orbital time scale and new C-isotope record for Cenomanian–Turonian boundary stratotype. Geology 34, 125.
Sames, B., Wagreich, M., Wendler, J.E., Haq, B.U., Conrad, C.P., Melinte-Dobrinescu, M.C., Hu, X., Wendler, I., Wolfgring, E., Yilmaz, I.Ö., Zorina, S.O., 2016. Review: short-term sea-level changes in a greenhouse world — a view from the Cretaceous. Palaeogeogr. Palaeoclimatol. Palaeoecol. 441, 393–411. https://doi.org/10.1016/j.palaeo.2015.10.045.
Savrda, C.E., 1998. Ichnology of the Bridge Creek Limestone: evidence for temporal and spatial variations in paleo-oxygenation in the Western Interior Seaway, in Dean, W.E., and Arthur, M.A., eds., Stratigraphy and Paleoenvironments of the Cretaceous Western Interior Seaway, U.S.A., SEPM. Concepts in Sedimentology and Paleontology 6, 127–136.
Schlanger, S., Jenkyns, H., 1976. Cretaceous oceanic anoxic events: causes and consequences. Geol. Mijnb. 55, 179–184.
Scholle, P.A., Arthur, M.A., 1980. Carbon isotope fluctuations in Cretaceous pelagic limestones: potential stratigraphic and petroleum exploration tool. AAPG Bull. 64, 67–87.
Schubert, B.A., Jahren, A.H., 2012. The effect of atmospheric CO_2 concentration on carbon isotope fractionation in C3 land plants. Geochim. et Cosmochim. Acta 96, 29–43.
Schulz, M., Schäfer-Neth, C., 1997. Translating Milankovitch climate forcing into eustatic fluctuations via thermal deep water expansion: a conceptual link. Terra Nova 9, 228–231. https://doi.org/10.1111/j.1365-3121.1997.tb00018.x.
Scotese, C. R., 2001. Atlas of Earth History, Volume 1, Paleogeography, PALEOMAP Project, Arlington, Texas, 52 pp.
Sinninghe Damsté, J.S., Kuypers, M.M.M., Pancost, R.D., Schouten, S., 2008. The carbon isotopic response of algae, (cyano)bacteria, archaea and higher plants to the late Cenomanian perturbation of the global carbon cycle: insights from biomarkers in black shales from the Cape Verde Basin (DSDP Site 367). Org. Geochem. 39, 1703–1718.
Sinninghe Damsté, J.S., van Bentum, E.C., Reichart, G.-J., Pross, J., Schouten, S., 2010. A CO_2 decrease-driven cooling and increased latitudinal temperature gradient during the mid-Cretaceous Oceanic Anoxic Event 2, Earth Planet. Sci. Lett. 293, 97–103. https://doi.org/10.1016/j. epsl.2010.02.027.
Smedley, M.P., Dawson, T.E., Comstock, J.P., Donovan, L.A., Sherrill, D.E., Cook, C.S., Ehleringer, J.R., 1991. Seasonal carbon isotope discrimination in a grassland community. Oecologia 85, 314–320.
Snow, L.J., Duncan, R.A., Bralower, T.J., 2005. Trace element abundances in the Rock Canyon Anticline, Pueblo, Colorado, marine sedimentary section and their relationship to Caribbean plateau construction and oxygen anoxic event 2. Paleoceanography 20, PA3005. https://doi.org/10.1029/2004PA001093.
Steinthorsdottir, M., Woodward, F.I., Surlyk, F., McElwain, J.C., 2012. Deep-time evidence of a link between elevated CO_2 concentrations and perturbations in the hydrological cycle via drop in plant transpiration. Geology 40 (9), 815–818.
Takashima, R., Nishi, H., Yamanaka, T., Hayashi, K., Waseda, A., Obuse, A., Tomosugi, T., Deguchi, N., Mochizuki, S., 2010. High-resolution terrestrial carbon isotope and planktic foraminiferal records of the Upper Cenomanian to the Lower Campanian in the Northwest Pacific. Earth Planet. Sci. Lett. 289, 570–582.
Tibert, N. E., Leckie, R. M., Eaton, J. G., Kirkland, J. I., Colin, J.-P., Leithold, E. L., and Mccormic, M. E., 2003, Recognition of relative sea-level change in Upper Cretaceous coal-bearing strata: a paleoecological approach using agglutinated Foraminifera and ostracodes to detect key stratigraphic surfaces, in C, O. H., and Leckie, R. M., eds., Micropaleontologic proxies for sea-level change and stratigraphic discontinuities, Volume 75, Society for Sedimentary Geology, p. 263–299.
Toft, N.L., Anderson, J.E., Nowak, R.S., 1989. Water use efficiency and carbon isotope composition of plants in a cold desert environment. Oecologia 80, 11–18.
Trabucho Alexandre, J., Tuenter, E., Henstra, G.A., van der Zwan, K.J., van de Wal, R.S.W., Dijkstra, H.A., de Boer, P.L., 2010. The mid-Cretaceous North Atlantic nutrient trap: black shales and OAEs. Paleoceanography 25, PA4201. https://doi.org/10.1029/2010PA001925.
Tsikos, H., Jenkyns, H.C., Walsworth-Bell, B., Petrizzo, M.R., Forster, A., Kolonic, S., Erba, E., Premoli Silva, I., Baas, M., Wagner, T., Sinninghe Damsté, J.S., 2004. Carbon-isotope stratigraphy recorded by the Cenomanian-Turonian Oceanic Anoxic Event: correlation and implications based on three key localities. J. Geol. Soc. Lond. 161, 711–719.
Turgeon, S.C., Creaser, R.A., 2008. Cretaceous Anoxic Event 2 triggered by a massive magmatic episode. Nature 454, 323–326.
Uličný, D., 1999. Sequence stratigraphy of the Dakota Formation (Cenomanian), southern Utah: interplay of eustasy and tectonics in a foreland basin. Sedimentology 46 (5), 807–836.
van Helmond, N.A.G.M., Sluijs, A., Reichart, G.-J., Sinninghe Damsté, J.S., Slomp, C.P., Brinkhuis, H., 2014. A perturbed hydrological cycle during Oceanic Anoxic Event 2. Geology 42, 123–126. https://doi.org/10.1130/G34929.1.
van Helmond, N.A.G.M., Sluijs, A., Sinninghe Damsté, J.S., Reichart, G.-J., Voigt, S., Erbacher, J., Pross, J., Brinkhuis, H., 2015. Freshwater discharge controlled deposition of Cenomanian–Turonian black shales on the NW European epicontinental shelf (Wunstorf, northern Germany). Clim. Past 11, 495–508. https://doi.org/10.5194/cp-11-495-2015.
Wagreich, M., Lein, R., Sames, B., 2014. Eustasy, its controlling factors, and the limno-eustatic hypothesis — concepts inspired by Eduard Suess. J. Aust. Earth Sci. 107 (1), 115–131.
Wendler, J.E., Meyers, S.R., Wendler, I., Kuss, J., 2014. A million-year-scale astronomical control on Late Cretaceous sea-level. Newsl. Stratigr. 47, 1–19. https://doi.org/10.1127/0078-0421/2014/0038.

Wendler, J.E., Wendler, I., Vogt, C., Kuss, J., 2016. Link between cyclic eustatic sea-level change and continental weathering: evidence for aquifer-eustasy in the Cretaceous. Palaeogeogr. Palaeoclimatol. Palaeoecol. 441, 430–437.

Wright, G.C., Nageswara Rao, R.C., Farquhar, G.D., 1994. Water-use efficiency and carbon isotope discrimination in peanut under water deficit conditions. Crop Sci. 34, 92–97.

Wynn, J.G., 2007. Carbon isotope fractionation during decomposition of organic matter in soils and paleosols: Implications for paleoecological interpretations of paleosols. Palaeogeogr. Palaeoclimatol. Palaeoecol. 251, 437–448.

Xing, L., Zhang, H., Yuan, Z., Sun, Y., Zhao, M., 2011. Terrestrial and marine biomarker estimates of organic matter sources and distributions in surface sediments from the East China Seashelf. Cont. Shelf Res. 31, 1106–1115.

Zeebe, R.E., 2012. History of seawater carbonate chemistry, atmospheric CO_2, and ocean acidification. Annu. Rev. Earth Planet. Sci. 40, 141–165.

Zeebe, R.E., Westerhold, T., Littler, K., Zachos, J.C., 2017. Orbital forcing of the Paleocene and Eocene carbon cycle. Paleoceanography 32, 440–465. https://doi.org/10.1002/2016PA003054.